Solitary Waves and Enhanced Incoherent Scatter Ion Lines

Jonas Ekeberg

Solitary Waves and Enhanced Incoherent Scatter Ion Lines

JONAS EKEBERG

Akademisk avhandling som med vederbörligt tillstånd av Rektor vid Umeå universitet för avläggande av teknologie doktorsexamen i rymdfysik framläggs till offentligt försvar i aulan vid Institutet för rymdfysik, Rymdcampus 1, Kiruna, fredagen den 13 maj, kl. 10.00. Avhandlingen kommer att försvaras på engelska.

Fakultetsopponent: Prof. Jan Trulsen, Institutt for teoretisk astrofysikk, Universitetet i Oslo

Solitary Waves and Enhanced Incoherent Scatter Ion Lines

JONAS EKEBERG

Doctoral Thesis
Kiruna, Sweden, 2011

Jonas Ekeberg
Swedish Institute of Space Physics, Box 812, SE-981 28 Kiruna, Sweden

IRF Scientific Report 301
ISSN 0284-1703
ISBN 978-91-977255-7-6

© Jonas Ekeberg, 2011

Printed in Sweden by Aurells Tryckeri AB, Västerås, 2011

Till Morfar

Abstract

This thesis addresses solitary waves and their significance for auroral particle acceleration, coronal heating and incoherent scatter radar spectra. Solitary waves are formed due to a balance of nonlinear and dispersive effects. There are several nonlinearities present in ideal magnetohydrodynamics (MHD) and dispersion can be introduced by including the Hall term in the generalised Ohm's law. The resulting system of equations comprise the classical ideal MHD waves, whistlers, drift waves and solitary wave solutions. The latter reside in distinct regions of the phase space spanned by the speed and the angle (to the magnetic field) of the propagating wave. Within each region, qualitatively similar solitary structures are found. In the limit of neglected electron intertia, the solitary wave solutions are confined to two regions of slow and fast waves, respectively. The slow (fast) structures are associated with density compressions (rarefactions) and positive (negative) electric potentials. Such negative potentials are shown to accelerate electrons in the auroral region (solar corona) to tens (hundreds) of keV. The positive electric potentials could accelerate solar wind ions to velocities of 300–800 km/s. The structure widths perpendicular to the magnetic field are in the Earth's magnetosphere (solar corona) of the order of 1–100 km (m). This thesis also addresses a type of incoherent scatter radar spectra, where the ion line exhibits a spectrally uniform power enhancement with the up- and downshifted shoulder and the spectral region in between enhanced simultaneously and equally. The power enhancements are one order of magnitude above the thermal level and are often localised to an altitude range of less than 20 km at or close to the ionospheric F region peak. The observations are well-described by a model of ion-acoustic solitary waves propagating transversely across the radar beam. Two cases of localised ion line enhancements are shown to occur in conjunction with auroral arcs drifting through the radar beam. The arc passages are associated with large gradients in ion temperature, which are shown to generate sufficiently high velocity shears to give rise to growing Kelvin-Helmholtz (K-H) instabilities. The observed ion line enhancements are interpreted in the light of the low-frequency turbulence associated with these instabilities.

KEYWORDS: plasma waves and instabilities, nonlinear phenomena, solitons and solitary waves, ionosphere, Sun: corona, incoherent scatter radar, MHD

Sammanfattning

Denna avhandling handlar om solitära vågor och deras roll i norrskensacceleration och koronauppheттning, samt deras signatur i spektra uppmätta med inkoherent spridningsradar. Solitära vågor bildas genom en balans mellan ickelinjära och dispersiva effekter. Ickelinjäriteter finns det gott om i ideal magnetohydrodynamik (MHD) och dispersion kan införas genom att inkludera Halltermen i den generaliserade Ohms lag. Det resulterande ekvationssystemet omfattar de klassiska vågorna inom ideal MHD, visslare, driftvågor och solitära vågor. De sistnämnda återfinns i väldefinierade områden i fasrummet som spänns upp av farten och vinkeln (mot magnetfältet) för den propagerande vågen. Inom varje sådant område återfinns kvalitativt lika solitära våglösningar. Om man försummar elektronernas tröghet begränsas de solitära våglösningarna till två områden med långsamma respektive snabba vågor. De långsamma (snabba) strukturerna är associerade med täthets-kompressioner (förtunningar) och positiva (negativa) elektriska potentialer. De negativa potentialerna visas kunna accelerera elektroner i norrskensområdet (solens korona) till tiotals (hundratals) keV medan de positiva potentialerna accelererar solvindsjoner till hastigheter på 300–800 km/s. Strukturbredderna vinkelrät mot magnetfältet är i jordens magnetosfär (solens korona) av storleksordningen 1–100 km (m). Denna avhandling tar även upp en typ av inkoherent spridningsradarspektra, där jonlinjen uppvisar en spektralt uniform förstärkning. Detta innebär att den upp- och nedskiftade skuldran och spektralbandet däremellan förstärks simultant och i lika hög grad. Effektförstärkningen är en storleksordning över den termiska nivån och är ofta lokaliserad till ett höjd-intervall av mindre än 20 km nära jonosfärens F-skiktstopp. Observationerna beskrivs väl av en modell med solitära vågor som propagerar transversellt genom radarstrålen. Två fall av lokaliserade jonlinjeförstärkningar visas sammanfalla med att norrskensbågar driver genom radarstrålen. I samband med bågarnas passage uppmäts stora gradienter i jontemperatur, vilket visas skapa tillräckligt kraftiga hastighetsskjuvningar för att Kelvin-Helmholtz-instabiliteter ska tillåtas växa. De observerade jonlinjeförstärkningarna tolkas i skenet av den lågfrekventa turbulensen som är kopplad till dessa instabiliteter.

NYCKELORD: plasmavågor och instabiliteter, ickelinjära fenomen, solitoner och solitära vågor, jonosfär, solen: korona, inkoherent spridningsradar, MHD

List of included papers

This thesis is based on the following papers, which are referred to in the text by their Roman numerals.

I Stasiewicz, K. & Ekeberg, J. Dispersive MHD waves and alfvenons in charge non-neutral plasmas. (2008). *Nonlin. Proc. Geophys.*, *15*, 681–693.

II Stasiewicz, K. & Ekeberg, J. Electric Potentials and Energy Fluxes Available for Particle Acceleration by Alfvenons in the Solar Corona. (2008). *Astrophys. J. Lett.*, *680*, L153–L156.

III Stasiewicz, K. & Ekeberg, J. Heating of the Solar Corona by Dissipative Alfvén Solitons - Reply. (2007). *Phys. Rev. Lett.*, *99*(8), 89502.

IV Ekeberg, J., Wannberg, G., Eliasson, L., & Stasiewicz, K. (2010). Ion-acoustic solitary waves and spectrally uniform scattering cross section enhancements, *Ann. Geophys.*, *28*(6), 1299–1306.

V Ekeberg, J., Wannberg, G., Eliasson, L., & Häggström, I. (2011). Soliton-induced spectrally uniform ion line power enhancements at the ionospheric *F* region peak. Submitted to *Earth Planets Space*.

VI Ekeberg, J., Stasiewicz, K., Wannberg, G., Sergienko, T., & Eliasson, L. (2011). Incoherent scatter ion line enhancements and auroral arc-induced Kelvin-Helmholtz turbulence. Submitted to *J. Atmos. Solar-Terr. Phys.*.

The papers have been reproduced by permission of the publishers.

List of papers not included in the thesis

- Belova, E., Kirkwood, S., Ekeberg, J., Osepian, A., Häggström, I., Nilsson, H., & Rietveld, M. The dynamical background of polar mesospheric winter echoes from simultaneous EISCAT and ESRAD observations. (2005). *Ann. Geophys.*, *23*(4), 1239–1247.

- Kirkwood, S., Belova, E., Chilson, P., Dalin, P., Ekeberg, J., Häggström, I., & Osepian, A. ESRAD / EISCAT Polar Mesosphere Winter Echoes during Magic and Roma. (2005). *Proceedings of the 17th ESA Symposium on European Rocket and Balloon Programmes and Related research*, Sandefjord, Norway, 30 May- 2 June 2005, ESA-SP-590, 115-119.

Contents

CHAPTER 1

Introduction

In addition to the solid, liquid and gas states, *plasma* is sometimes referred to as the fourth state of matter (e.g. Clemmow and Dougherty, 1969). The plasma state is achieved by significant heating of a gas so that electrons separate from the atomic nuclei, resulting in a partly ionised medium. This medium will respond to electromagnetic fields, which introduce new dynamics and additional phenomena compared to those found in neutral gases.

More than 99% of the visible matter in the universe is thought to be in the plasma state and plasma occurrences cover distant stars gleaming on a clear night, flickering *aurora borealis* (northern lights) and lively campfires. Industrial products and applications involving plasmas include plasma screens, metals processing, and thermonuclear fusion. Figure 1.1 provides some more examples and relates them to typical temperature and density ranges. As is evident from the figure, plasmas occupy a vast region of the temperature-density parameter space. An interesting consequence of this is that plasma phenomena first acknowledged in one area of plasma physics often have a useful equivalent in other areas. In this sense, there is much to be gained from exchange of ideas between plasma physicists, regardless of whether the experimentalists in the respective fields utilise telescopes, *in-situ* satellite measurements or fusion test reactors.

Since a plasma is an ionised gas and we know from everyday life that neutral fluid mediums such as oceans and gases mediate different types of waves, it is not surprising that such phenomena have their equivalents in plasmas, with additional dynamics provided by the electromagnetic fields. This thesis addresses different types of such plasma waves, and focuses on a particular type, namely exponentially growing solitary waves. This type of plasma wave is studied in the context of acceleration processes in the solar corona and in the Earth's magnetosphere.

Another significant part of this thesis addresses enhanced incoherent scatter radar spectra and introduces a mechanism of ion-acoustic solitary waves enhancing the radar cross section, is introduced. Another suggested mechanism for the observed spectra is the turbulence associated with auroral arcs passing through

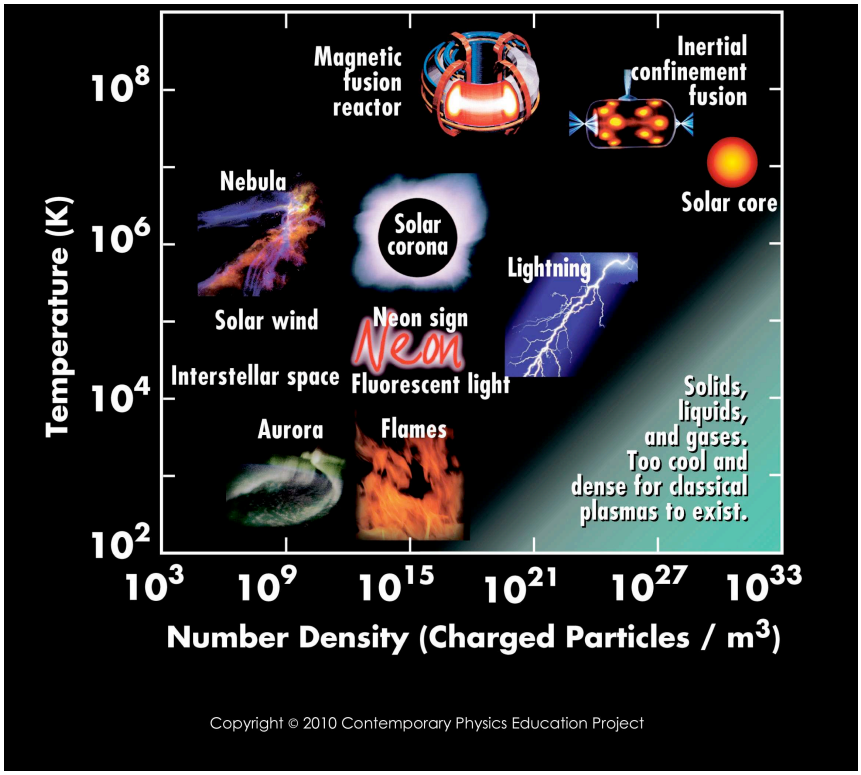

Figure 1.1. Occurrences of plasmas in terms of typical densities and temperatures. The figure is adopted with kind permission from the Contemporary Physics Education Project.

the radar beam.

This thesis comprises two parts: a collection of six papers and a summary of the topics addressed in the papers. Chapter 2 presents the basic plasma concepts and provides a foundation for Chapter 3, which discusses various plasma models. Chapter 4 describes a method of describing plasma waves and comments on the stationary wave frame, where solitary waves are studied. Chapter 5 introduces the concept of an ionosphere and its associated plasma component. This is the environment where incoherent scatter radars operate and the spectra derived from such measurements are described in Chapter 6. The last chapter contains short summaries of the included papers, which are attached at the end of the thesis.

1.1 Notation and constants

SI units have been used throughout the thesis. Italics are used for variables, bold for vectors and sans serif for tensors. The symbol '$\hat{}$' is used to denote unit vectors, so $\hat{\mathbf{v}} = \mathbf{v}/|\mathbf{v}|$. Subscripts are used to denote Cartesian vector components (x, y, z), directions relative to magnetic field ($\perp$ and $\parallel$) and particle species (e for electron, i for ion and α for arbitrary species). Variables and constants (Nordling and Österman, 1996) utilised in the thesis are listed below.

Variables

$\mathbf{B}$	magnetic field
$\mathbf{E}$	electric field
P	pressure tensor
T	temperature
m	mass of particle
q	electric charge of particle
$\mathbf{x}$	position
$\mathbf{v}$	velocity
$\mathbf{X}$	phase space variable; $(\mathbf{x}, \mathbf{v})$
ρ	charge density
$\mathbf{J}$	current density
N	number of particles in a system
n	number of particles per unit volume $\left(N = \int n(t, \mathbf{x})\, \mathrm{d}\mathbf{x}\right)$
ν	number of degrees of freedom in a system
$C_{p(v)}$	heat capacity at constant pressure (volume)
$\gamma = C_p/C_v$	polytropic index
Λ_D	the Debye length
g	the plasma parameter
β	plasma beta
l	characteristic length scale
τ	characteristic time scale
$v_{\mathrm{th},\alpha} = \sqrt{2k_\mathrm{B}T_\alpha/m_\alpha}$	thermal (most probable) speed of species α
$r_\alpha = v_{\perp\alpha}/\omega_{\mathrm{c}\alpha}$	cyclotron radius (gyroradius, Larmor radius) of species α
$\omega_{\mathrm{c}\alpha} = \lvert q_\alpha \rvert B/m_\alpha$	cyclotron frequency (gyrofrequency) of species α
$\omega_{\mathrm{p}\alpha} = \sqrt{nq_\alpha^2/\varepsilon_0 m_\alpha}$	plasma frequency of species α
$\lambda_\alpha = c/\omega_{\mathrm{p}\alpha}$	inertial length of species α
V_A	Alfvén speed
c_s	ion-acoustic speed

Constants

Symbol	Quantity	Value	Unit
c	speed of light in vacuum	2.99792458×10^{8}	m/s
ε_0	permittivity of free space	$8.8541878 \times 10^{-12}$	As/Vm
μ_0	permeability of free space	$4\pi \times 10^{-7}$	Vs/Am
m_e	electron mass	9.109390×10^{-31}	kg
u	atomic mass unit	1.66054×10^{-27}	kg
e	elementary charge	$1.6021773 \times 10^{-19}$	C
k_B	Boltzmann constant	1.38066×10^{-23}	J/K

CHAPTER 2

Basic plasma concepts

The term *plasma* was first used by Langmuir (1928) and Tonks and Langmuir (1929) to describe a region containing balanced charges of ions and electrons. Although the term had already been used in physiology since the previous century to describe the clear fluid constituent in blood, the similarities end there. In contrast to the plasma in blood, where it transports the corpuscular material, there is no such medium for the electrons, ions, and neutrals in ionised gases. However, Lord Rayleigh had already pinpointed the collective behaviour of the charged particles in a plasma. In his study of electron oscillations in the Thomson model of the atom, he treated the electron cloud surrounding the core as a continuous electron fluid (Lord Rayleigh., 1906). This thesis and the papers included in it are based on such a treatment for both the electrons and the ions.

This chapter gives a brief introduction to some of the most fundamental concepts in plasma physics.

2.1 Debye shielding

The electrostatic potential $\phi(r)$ at a distance r from a test particle of charge q in vacuum is

$$\phi(r) = \frac{1}{4\pi\varepsilon_0}\frac{q}{r}. \tag{2.1}$$

Inserting such a test particle in a spatially uniform and neutral plasma will attract and repel particles of similar and opposite polarities, respectively. The attracted particles will partially cancel the test particle potential, a process called *shielding* or *screening*. The resulting potential, the Yukawa potential, is given by

$$\phi(r) = \frac{1}{4\pi\varepsilon_0}\frac{q}{r}e^{-r/\Lambda_D}, \tag{2.2}$$

where Λ_D is the Debye length, a concept originating from the theory of electrolytes (Debye and Hückel, 1923). It is defined in terms of the species' Debye lengths $\Lambda_{D\alpha}$

according to

$$\frac{1}{\Lambda_D^2} = \sum_\alpha \frac{1}{\Lambda_{D\alpha}^2} \tag{2.3}$$

$$\Lambda_{D\alpha} = \sqrt{\frac{\varepsilon_0 k_\mathrm{B} T_\alpha}{n_\alpha q_\alpha^2}}. \tag{2.4}$$

A small (large) Debye length corresponds to a rapidly (slowly) decaying potential with distance from a test charge. In other words, a species with a small Debye length will effectively shield a test charge. However, because of the large difference in inertia between electrons and ions, only electrons can keep up with and provide shielding for other electrons, whereas ions are shielded by both electrons and ions.

2.2 The plasma approximation

In order for the shielding concept in Section 2.1 to make sense, a large number of plasma particles are required in the shielding cloud of radius Λ_D, which introduces the plasma parameter g defined by (e.g. Krall and Trivelpiece, 1973)

$$g = \frac{1}{n\Lambda_D^3} \sim \frac{n^{1/2}}{T^{3/2}}, \tag{2.5}$$

where (2.3) and (2.4) were inserted. The assumption of many particles in the Debye sphere corresponds to $g \ll 1$ and is called the *plasma approximation*, where collective behaviour dominates over the effects of individual particles. Since the collision frequency decreases with decreasing density and increasing temperature, it is seen from (2.5) that $g \to 0$ corresponds to a low collision frequency. The Debye length must also be small compared to the plasma dimensions in order for sufficiently many particles to be outside the shielding cloud.

2.3 Quasineutrality

When introducing the concept of Debye shielding, the plasma was assumed to be initially charge neutral. It can be shown (e.g. Bellan, 2006) that plasmas to a large extent remain close to, but not exactly, neutral on scale lengths much larger than the Debye length. This is because a plasma in general does not have sufficient internal energy to generate large-scale non-neutralities. This behaviour is often referred to as *quasineutrality*.

2.4 Magnetic pressure

A plasma is by nature diamagnetic, i.e. it will act repulsively to external magnetic fields. Therefore, a magnetic pressure can balance the kinetic pressure of the plasma at a boundary between a plasma and a magnetic field. This is utilized in magnetic confinement fusion, where the magnetic field prevents the plasma from cooling at the surrounding walls and can be used to heat the plasma through compression (e.g. Chen, 1984). In order to quantify the relative importance of the kinetic and magnetic pressures, the parameter *plasma beta* is introduced;

$$\beta = \sum_{\alpha} \beta_{\alpha}, \text{ where } \beta_{\alpha} = \frac{n_{\alpha} k_B T_{\alpha}}{B^2/2\mu_0}. \tag{2.6}$$

As will be shown later, β is a useful measure in qualitative plasma assessment.

2.5 Inertial lengths

Besides the radii of the gyration motion performed by electrons and ions subject to a magnetic field, the electron and ion *inertial lengths* (skin depths) are two other important length scales in plasma physics. The inertial length for species α is given by

$$\lambda_{\alpha} = \frac{c}{\omega_{\mathrm{p}\alpha}} = \sqrt{\frac{m_{\alpha}}{\mu_0 n_{\alpha} q_{\alpha}^2}} \tag{2.7}$$

and is a measure of the penetration depth of an electromagnetic wave propagating into a plasma.

2.6 Particle motion in a uniform magnetic field

Consider a charged particle of mass m_{α}, charge q_{α} and velocity $\mathbf{v}_{\alpha}$ in a uniform magnetic field $\mathbf{B}$ in the absence of other fields. The equation of motion is given by

$$m_{\alpha} \frac{\mathrm{d}\mathbf{v}_{\alpha}}{\mathrm{d}t} = q(\mathbf{v}_{\alpha} \times \mathbf{B}), \tag{2.8}$$

where $\mathbf{v}_{\alpha}$ can be split into a parallel (to $\mathbf{B}$) and a perpendicular part. Thus, we have

$$m \frac{\mathrm{d}\mathbf{v}_{\alpha\parallel}}{\mathrm{d}t} = \mathbf{0} \tag{2.9}$$

$$m \frac{\mathrm{d}\mathbf{v}_{\alpha\perp}}{\mathrm{d}t} = q(\mathbf{v}_{\alpha\perp} \times \mathbf{B}). \tag{2.10}$$

It is seen that the motion along $\mathbf{B}$ is constant and the last equation is recognized as a central motion, thus

$$|q_\alpha| \, v_{\alpha\perp} B = \frac{m v_{\alpha\perp}^2}{r_\alpha} \tag{2.11}$$

$$\Leftrightarrow r_\alpha = \frac{m v_{\alpha\perp}}{|q_\alpha| \, B}, \tag{2.12}$$

where r_α is the *cyclotron radius* (*gyroradius, Larmor radius*). The corresponding *cyclotron frequency* (*gyrofrequency*) is given by

$$\omega_{\mathrm{c}\alpha} = \frac{v_\perp}{r_\alpha} = \frac{|q_\alpha| \, B}{m_\alpha}. \tag{2.13}$$

It can be seen from (2.8) that positive (negative) charges will gyrate in a left-handed (right-handed) fasion with respect to the magnetic field. By including additional fields and forces, such as an electric field, gravity or pressure gradients, the resulting charged particle motion will be a gyration around a drifting centre. This concept of guiding-centre motion was developed by Alfvén (1953).

2.7 Plasma frequency

In addition to the gyro frequencies, the *plasma frequency* is a fundamental timescale in plasma physics. Because a plasma consists of charged particles exerting long-range forces, it can be viewed as a system of coupled oscillators.

Consider a two-species quasineutral plasma of electrons and ions and let a group of electrons be displaced slightly from their equilibrium position $\mathbf{x}_0$. This will set up an electric field, which forces them back to $\mathbf{x}_0$. However, upon returning to $\mathbf{x}_0$, the group of electrons will have gained a kinetic energy equal to the potential energy of their displacement. They will therefore overshoot $\mathbf{x}_0$ and continue their movement until their kinetic energy is converted back to potential energy, which is followed by an overshoot in the other direction, etc. The inertial frequency of this harmonic oscillation in a quasineutral plasma is the plasma frequency, which for species α is given by

$$\omega_{\mathrm{p}\alpha} = \sqrt{\frac{n q_\alpha^2}{\varepsilon_0 m_\alpha}}. \tag{2.14}$$

CHAPTER 3

Vlasov-, two-fluid-, and MHD models

The properties and processes in a plasma can be described either macroscopically (fluid) or microscopically (kinetic). Whereas the macroscopic approach describes measurable quantities such as average velocity and temperature, the microscopic description is based on the velocity-space distribution of the particles and describes their associated microfields and interactions. Such interaction processes include collisions and scattering of radiation by a plasma. This chapter introduces model equations of both types as well as the approximations upon which they rest.

3.1 Vlasov theory

A complete microscopic description of a plasma with N_α particles of type α, N_β particles of type β, ..., and N_γ particles of type γ is one where the spatial coordinates $\mathbf{x}_i(t)$ and velocities $\mathbf{v}_i(t)$ of each particle $i = 1, 2, ..., N_\alpha + N_\beta + ... + N_\gamma$ are given as functions of time. These are given by the equations of motion for each particle. If all other forces but the electromagnetic are neglected, the equations read

$$\frac{\mathrm{d}\mathbf{x}_i}{\mathrm{d}x} = \mathbf{v}_i \tag{3.1}$$

$$\frac{\mathrm{d}\mathbf{v}_i}{\mathrm{d}x} = \frac{q_i}{m_i}\left(\mathbf{E}^{\mathrm{M}} + \mathbf{v}_i \times \mathbf{B}^{\mathrm{M}}\right), \tag{3.2}$$

where $\mathbf{E}^{\mathrm{M}}$ and $\mathbf{B}^{\mathrm{M}}$ are the microscopic fields due to all particles except for the ith. Solving these microscopic equations for all particles is a strenuous task. Instead, the statistical properties of the system above are determined by the distribution of its particles in the six-dimensional phase space $\mathbf{X} = (\mathbf{x}, \mathbf{v})$. The system has a probability density $F = F(\mathbf{X}_{\alpha 1}, ..., \mathbf{X}_{\alpha N_\alpha}, \mathbf{X}_{\beta 1}, ..., \mathbf{X}_{\beta N_\beta}, ..., \mathbf{X}_{\gamma 1}, ..., \mathbf{X}_{\gamma N_\gamma}, t)$ such that

$$F\mathrm{d}\mathbf{X}_{\alpha 1}\mathrm{d}\mathbf{X}_{\alpha 2}\cdots\mathrm{d}\mathbf{X}_{\alpha N_\alpha}\mathrm{d}\mathbf{X}_{\beta 1}\cdots\mathrm{d}\mathbf{X}_{\beta N_\beta}\cdots\mathrm{d}\mathbf{X}_{\gamma 1}\cdots\mathrm{d}\mathbf{X}_{\gamma N_\gamma} \equiv F\mathrm{d}X_{\mathrm{all}} \tag{3.3}$$

is the probability that at time t finding the particles in the respective ranges $[\mathbf{X}_{\xi i}, \mathbf{X}_{\xi i} + \mathrm{d}\mathbf{X}_{\xi i}], \forall_{\xi,i}$. Consequently,

$$\int F \, \mathrm{d}X_{\mathrm{all}} = 1. \tag{3.4}$$

By integrating the probablity density F over coordinates of all but some particles, reduced distributions are obtained. These are more straightforward to study than F but are less accurate. For example, a one-particle distribution function is calculated by integrating over all coordinates except for those of the particle according to

$$f_\alpha(\mathbf{X}_{\alpha 1}, t) = N_\alpha \int F \, \frac{\mathrm{d}\mathbf{X}_{\mathrm{all}}}{\mathrm{d}\mathbf{X}_{\alpha 1}}. \tag{3.5}$$

Thus, $f_\alpha(\mathbf{X}, t)/N_\alpha \, \mathrm{d}\mathbf{X}$ is the probability of finding a particle of type α at time t in the range $[\mathbf{X}, \mathbf{X} + \mathrm{d}\mathbf{X}]$. This distribution does not include any effects of neighbouring particles. While, in contrast to F, it is often possible to guess the shape of $f_\alpha(\mathbf{x}, \mathbf{v}, t)$ at $t = 0$, knowledge of its time evolution is desirable. This can be calculated from the *Klimontovich-Dupree equation* (Dupree, 1963; Klimontovich, 1967; Krall and Trivelpiece, 1973). However, calculating the evolution of f_α requires knowledge of $f_{\alpha\beta}$, which in turn depends on $f_{\alpha\beta\gamma}$ etc. These higher-order distribution functions can be expressed in terms of one-particle distributions and their correlations (Krall and Trivelpiece, 1973):

$$\begin{aligned} f_{\alpha\beta} &= f_\alpha f_\beta + \varrho_{\alpha\beta} \\ f_{\alpha\beta\gamma} &= f_\alpha f_\beta f_\gamma + f_\alpha \varrho_{\beta\gamma} + f_\beta \varrho_{\alpha\gamma} + f_\gamma \varrho_{\alpha\beta} + \varrho_{\alpha\beta\gamma} \\ &\vdots \end{aligned} \tag{3.6}$$

ϱ is the correlation between the subscripted particle species, thus statistically independent particles have $\varrho = 0$.

It was shown in Section 2.2 that the plasma approximation requires the plasma parameter g to be small, i.e. the Debye length to be much greater than the interparticle spacing. The terms in (3.6) can be expanded as a series in g:

$$\begin{aligned} f_\alpha &\sim \mathcal{O}(1) \\ \varrho_{\alpha\beta} &\sim \mathcal{O}(g) \\ \varrho_{\alpha\beta\gamma} &\sim \mathcal{O}(g^2) \\ &\vdots \end{aligned} \tag{3.7}$$

Neglecting all terms of order g, it can be shown (e.g. Krall and Trivelpiece, 1973) that the evolution of the distribution function f_α for species α with charge q_α and mass m_α under influence of only the electromagnetic force is given by

$$\frac{\partial f_\alpha}{\partial t} + \mathbf{v} \cdot \frac{\partial f_\alpha}{\partial \mathbf{x}} + \frac{q_\alpha}{m_\alpha} \left(\mathbf{E} + \mathbf{v} \times \mathbf{B} \right) \cdot \frac{\partial f_\alpha}{\partial \mathbf{v}} = 0. \tag{3.8}$$

This is the *Vlasov equation* or *collisionless Boltzmann equation*, which is equivalent to $\mathrm{d}f_\alpha/\mathrm{d}t = 0$. Since there are no collisions, the distribution function is conserved. The particles interact through the average electric and magnetic fields, which are given by Maxwell's equations (Jackson, 1999):

$$\nabla \cdot \mathbf{E} = \rho/\varepsilon_0 \tag{3.9}$$

$$\nabla \cdot \mathbf{B} = 0 \tag{3.10}$$

$$\nabla \times \mathbf{E} = -\frac{\partial \mathbf{B}}{\partial t} \tag{3.11}$$

$$\nabla \times \mathbf{B} = \mu_0 \mathbf{J} + \varepsilon_0 \mu_0 \frac{\partial \mathbf{E}}{\partial t} \tag{3.12}$$

The macroscopic quantities number density n_α and mean velocity $\mathbf{u}_\alpha$ can be calculated as statistical moments of $f_\alpha = f_\alpha(\mathbf{x}, \mathbf{v}, t)$. Together with the charge density ρ and current density $\mathbf{J}$, they are defined below:

$$n_\alpha(\mathbf{x}, t) = \int f_\alpha \, \mathrm{d}\mathbf{v} \tag{3.13}$$

$$\mathbf{u}_\alpha(\mathbf{x}, t) = \frac{1}{n_\alpha} \int \mathbf{v} f_\alpha \, \mathrm{d}\mathbf{v} \tag{3.14}$$

$$\rho(\mathbf{x}, t) = \sum_\alpha q_\alpha n_\alpha \tag{3.15}$$

$$\mathbf{J}(\mathbf{x}, t) = \sum_\alpha q_\alpha n_\alpha \mathbf{u}_\alpha \tag{3.16}$$

An isolated system under the influence of collisions or other forms of randomisation will evolve towards the state of maximum entropy consistent with the conservation of total energy and total number of particles. This state is described by the *Maxwellian* distribution function

$$f_{\mathrm{M},\alpha}(\mathbf{x}, \mathbf{v}, t) = n_\alpha \left(\frac{m_\alpha}{2\pi k_B T_\alpha} \right)^{\nu/2} \exp\left[-\frac{m_\alpha \left(\mathbf{v} - \mathbf{u}_\alpha \right)^2}{2 k_B T_\alpha} \right], \tag{3.17}$$

where ν is the number of degrees of freedom. The Maxwellian distribution is applicable whenever the plasma is in thermal equilibrium.

3.2 Two-fluid plasma theory

There are various approximations of the Vlasov equation. The two-fluid equations comprise one such set of equations. They are obtained by calculating the zeroth and first order statistical moments of (3.8) resulting in the *continuity equation* and the *momentum equation*:

$$\frac{\partial n_\alpha}{\partial t} + \nabla \cdot (n_\alpha \mathbf{u}_\alpha) = 0 \tag{3.18}$$

$$n_\alpha m_\alpha \left[\frac{\partial \mathbf{u}_\alpha}{\partial t} + (\mathbf{u}_\alpha \cdot \nabla)\, \mathbf{u}_\alpha \right] = q_\alpha n_\alpha \left(\mathbf{E} + \mathbf{u}_\alpha \times \mathbf{B} \right) - \nabla \cdot \mathsf{P}_\alpha, \tag{3.19}$$

where the pressure tensor P_α was introduced. However, in all papers included in this thesis, the pressure tensor is assumed to be isotropic, thus only three identical diagonal terms remain and $\mathsf{P}_\alpha \rightarrow \nabla P_\alpha$. Together with Maxwell's equations (3.9)-(3.12), the system is closed with an equation of state for each species:

$$P_\alpha \propto n_\alpha^{\gamma_\alpha} \tag{3.20}$$

$$\gamma_\alpha = (\nu_\alpha + 2)/2, \tag{3.21}$$

where γ_α and ν_α are, respectively, the polytropic index and the number of degrees of freedom for species α undergoing adiabatic pressure changes (Mandl, 1988). $\gamma_\alpha = 1$ corresponds to isothermal pressure changes.

3.3 One-fluid plasma theory: Magnetohydrodynamics

In *magnetohydrodynamics* (MHD), the two fluids of electrons and ions, as described in Section 3.2, are reduced to a linear combination of the two. Assuming a plasma of electrons and single charged ions ($q_\mathrm{i} = -q_\mathrm{e} = e, m_\mathrm{i} \gg m_\mathrm{e}$) which is quasineutral ($n_\mathrm{i} \approx n_\mathrm{e} \approx n$), (3.18) and (3.19) give the MHD continuity equation, the MHD centre-of-mass momentum equation and the MHD *generalised Ohm's law*:

$$\frac{\partial n}{\partial t} + \nabla \cdot (n\mathbf{U}) = 0 \tag{3.22}$$

$$nm_i \left[\frac{\partial \mathbf{U}}{\partial t} + (\mathbf{U} \cdot \nabla)\, \mathbf{U} \right] = \mathbf{J} \times \mathbf{B} - \nabla P \tag{3.23}$$

$$\frac{m_e}{ne^2} \left[\frac{\partial \mathbf{J}}{\partial t} + \nabla \cdot \left(\mathbf{U}\mathbf{J} + \mathbf{J}\mathbf{U} - \mathbf{J}\mathbf{J}\frac{1}{ne} \right) \right] = \mathbf{E} + \mathbf{U} \times \mathbf{B} - \frac{1}{ne} \left(\mathbf{J} \times \mathbf{B} - \nabla P_\mathrm{e} \right), \tag{3.24}$$

where again the pressure tensors are assumed to be isotropic and the centre-of-mass velocity $\mathbf{U}$ is defined as

$$\mathbf{U} = \frac{\sum_\alpha m_\alpha n_\alpha \mathbf{u}_\alpha}{\sum_\alpha m_\alpha n_\alpha}. \tag{3.25}$$

Table 3.1. Validity for approximations which can be utilised in Ohm's law (3.24).

$\frac{m_\mathrm{e}}{ne^2}\left[\quad\right]$	can be neglected if	$\frac{l^2\omega_\mathrm{pe}^2}{c^2} \gg 1$
$\frac{1}{ne}\nabla P_\mathrm{e}$	can be neglected if	$\frac{l^2 m_\mathrm{e}\omega_\mathrm{ce}}{\tau k_\mathrm{B} T_\mathrm{e}} \gg 1$
$\frac{1}{ne}\left(\mathbf{J}\times\mathbf{B}\right)$	can be neglected if	$\frac{l^2\omega_\mathrm{pe}^2}{\tau c^2\omega_\mathrm{ce}} \gg 1$

The system is closed by an equation of state as in (3.20) and Maxwell's equations. Regarding the latter, (3.9) is replaced by quasineutrality and the displacement current in Ampère's law (3.12) can be neglected for non-relativistic speeds.

3.3.1 MHD approximations

The generalised Ohm's law (3.24) is, besides the assumption of quasineutrality and the mass approximation utilised above, often subject to several simplifications.

The most basic version of (3.24) is utilised in *ideal MHD*, where the ideal Ohm's law is given by $\mathbf{E}+\mathbf{U}\times\mathbf{B}=\mathbf{0}$. This is recognized as the Lorentz transformation of $\mathbf{E}$ to the frame moving with velocity $\mathbf{U}$ (Jackson, 1999) and implies that the magnetic flux is time-invariant in the frame of the plasma, a concept known as *frozen-in-flux*. The concept of frozen-in-flux is often accredited to Hannes Alfvén, although he also stressed that the concept could be highly misleading (e.g Alfvén, 1976, and references therein). The ideal MHD equations place restrictions on the typical length (time) scales l (τ) in the plasma such that (Bellan, 2006):

- the plasma is quasineutral, i.e. charge-neutral for $l \gg \Lambda_D$
- the speeds are non-relativistic, $l/\tau \ll c$
- the spatial scales are large, $l \gg \lambda_\mathrm{i}$
- the temporal scales are long, $\tau \gg 1/\omega_\mathrm{ci}$
- the pressure and density gradients are parallel.

The criteria for neglecting the terms in (3.24), which are absent in the ideal MHD Ohm's law, are given (Krall and Trivelpiece, 1973) in Table 3.1. The terms are listed in increasing order of significance for the ionospheric parameters utilised in Papers IV, V and VI. Consequently, the electron-inertia-term can be neglected in most cases.

3.3.2 Hall MHD

By neglecting the left hand side of (3.24), one retains what is called Hall MHD. The equation is identical to the formulation of Hassam and Huba (1988), who were preceded by formulations with cold ions and neglection of magnetic tension (Hassam and Lee, 1984; Hassam and Huba, 1987).

Through the inclusion of the Hall term $(ne)^{-1}\mathbf{J}\times\mathbf{B}$ in Ohm's law, the validity of ideal MHD is extended to spatial scales $l \gg \rho_{\rm e}, \rho_{\rm i}$ and $\rho_{\rm e} \ll l \ll \rho_{\rm i}$ and temporal frequencies $\omega \ll \omega_{\rm ci}, \omega_{ce}$ and $\omega_{\rm ci} \ll \omega \ll \omega_{\rm ce}$.

Regarding the concept of frozen-in-flux, it can be seen from (3.24) that Hall MHD is associated with a magnetic flux frozen into the electron fluid as opposed to ideal MHD, where the flux is frozen into the centre of mass fluid. It can further be shown that it is actually the sum of the magnetic flux and the vorticity ($\nabla\times\mathbf{U}$) which is frozen into the centre of mass fluid in Hall MHD (Hassam and Huba, 1988).

Hall MHD theory has received considerable interest since the late 1980's and has been assessed in various applications such as structuring of sub-Alfvénic plasma expansions, magnetic field transport in plasma switches for circuit breakers and in the context of magnetic reconnection. Refer to Huba (2003) and references therein for a good introduction to the subject. As we will see later in this thesis, the Hall term is also crucial for the generation of exponentially growing solitary waves.

3.3.3 Finite Larmor Radius effects

Electrons and ions will, as was shown in Chapter 2, gyrate in the presence of an external magnetic field. Because electrons and ions have different gyroradii, they will also be subject to different average forces. The assumption of isotropic pressure tensors in (3.23) and (3.24) is based on the assumption that such Finite Larmor Radius (FLR) effects can be neglected. This is justified if the representative spatial scales are large compared to the ion Larmor radius (Krall and Trivelpiece, 1973):

$$\frac{l\omega_{\rm ci}}{\sqrt{2k_{\rm B}T_{\rm i}/m_{\rm i}}} \gg 1 \tag{3.26}$$

With the ionospheric parameters of Paper IV, this condition corresponds to $l \gg 2$ m, which is fulfilled and FLR effects can be neglected. In the limit of $l \sim \rho_{\rm i}$, the anisotropic ion stress tensor should be retained (Roberts and Taylor, 1962).

Another way of examining the importance of FLR effects is by considering the ratio of ion gyro radius to ion inertial length, $\rho_{\rm i}/\lambda_{\rm i} = \sqrt{\beta_{\rm i}}$. Thus, FLR effects are particularly important in high-β plasmas.

3.3.4 Electron MHD

Electron MHD (EMHD) is a small-scale limit of (3.24) where $\lambda_e \lesssim l \ll \lambda_i$, $\omega_{ci} \ll \omega \lesssim \omega_{ce}$, and ions are considered to be a stationary neutralizing background while the electrons are the only source of inertia (Kingsep et al., 1990; Bulanov et al., 1992). Paper IV includes electron-inertial effects to first order and Paper II briefly discusses an effect of electron inertia relating to parallel (to the magnetic field) electric fields. In all other included papers, electron inertial effects have been neglected.

CHAPTER 4

Dispersion relations

This chapter introduces the procedure for deriving dispersion relations associated with linear plasma waves in general, and presents the waves associated with MHD fluid formalism in particular. These dispersion relations are then transformed to the stationary wave frame, where the waves are categorised as either sinusoidal or exponentially growing solitary waves. The two different classes are shown to reside in distinct regions of the phase space spanned by the speed and the angle (to the magnetic field) of the propagating wave.

4.1 The Alfvén wave

We start by deriving a fundamental plasma wave in fluid formalism. Assuming a cold plasma, $\nabla p = \mathbf{0}$, subject to ideal MHD, $\mathbf{E} + \mathbf{U} \times \mathbf{B} = \mathbf{0}$, Faraday's law (3.11) and Ampère's law (3.12), without displacement current, yield the following system of equations:

$$nm_i \left[\frac{\partial \mathbf{U}}{\partial t} + (\mathbf{U} \cdot \nabla)\, \mathbf{U} \right] = \frac{1}{\mu_0} (\nabla \times \mathbf{B}) \times \mathbf{B} \tag{4.1}$$

$$\frac{\partial \mathbf{B}}{\partial t} = \nabla \times (\mathbf{U} \times \mathbf{B}) \,. \tag{4.2}$$

This system is linearised by replacing each variable by a sum of a zero-indexed background value and a one-indexed small perturbation,

$$n = n_0 + \tilde{n}_1 \tag{4.3}$$

$$\mathbf{U} = \mathbf{0} + \tilde{\mathbf{U}}_1 \tag{4.4}$$

$$\mathbf{B} = B_0 \hat{\mathbf{z}} + \tilde{\mathbf{B}}_1, \tag{4.5}$$

and neglecting terms that involve products of perturbed quantities. Assuming perturbations in the form of plane waves, $\left\{ \tilde{n}_1, \tilde{\mathbf{U}}_1, \tilde{\mathbf{B}}_1 \right\} = \{ n_1, \mathbf{U}_1, \mathbf{B}_1 \}\, e^{\mathrm{i}(\mathbf{k}\cdot\mathbf{r} - \omega t)}$,

propagating parallel to the background magnetic field $\mathbf{B}_0$, the linearised system is given by

$$\frac{B_0}{\mu_0 n_0 m_\mathrm{i}} (\hat{\mathbf{z}} \times \mathbf{B}_1) \times \hat{\mathbf{z}} + \frac{\omega}{k} \mathbf{U}_1 = 0 \tag{4.6}$$

$$\frac{\omega}{k} \mathbf{B}_1 + B_0 \mathbf{U}_1 - B_0 U_{1z} \hat{\mathbf{z}} = 0. \tag{4.7}$$

The z-components of these equations imply that $U_{1z} = B_{1z} = 0$, while the remaining four components can be expressed as

$$\begin{pmatrix} \frac{B_0}{\mu_0 n_0 m_\mathrm{i}} & 0 & \omega/k & 0 \\ 0 & \frac{B_0}{\mu_0 n_0 m_\mathrm{i}} & 0 & \omega/k \\ \omega/k & 0 & B_0 & 0 \\ 0 & \omega/k & 0 & B_0 \end{pmatrix} \begin{pmatrix} B_{1x} \\ B_{1y} \\ U_{1x} \\ U_{1y} \end{pmatrix} = \begin{pmatrix} 0 \\ 0 \\ 0 \\ 0 \end{pmatrix}, \tag{4.8}$$

which has a non-trivial solution only if the determinant of the matrix is equal to zero. This condition gives a relation between the wave vector $\mathbf{k}$ and the angular frequency ω, a so called *dispersion relation*,

$$\left(\frac{\omega}{k}\right)^2 = \frac{B_0^2}{\mu_0 n_0 m_\mathrm{i}} \equiv V_A^2, \tag{4.9}$$

which describes a transverse wave propagating along a magnetic field line at the *Alfvén speed* V_A. It is seen that the phase velocity ω/k is independent of k, i.e. Alfvén waves are non-dispersive and all wavelengths propagate at the same speed.

4.2 The ion-acoustic wave

We wish to study the effect of a small adiabatic perturbation of the background density in an otherwise field-free plasma. Thus, the linearisation scheme is

$$\begin{aligned} n &= n_0 + \tilde{n}_1 && (4.10)\\ P &= P_0 + \tilde{P}_1 && (4.11)\\ \mathbf{U} &= \mathbf{0} + \tilde{\mathbf{U}}_1 && (4.12)\\ \mathbf{B} &= \mathbf{0} + \tilde{\mathbf{B}}_1 && (4.13) \end{aligned}$$

and an appropriate system of equations is given by

$$\begin{aligned} \frac{\partial n}{\partial t} + \nabla \cdot (n\mathbf{U}) &= 0 && (4.14)\\ nm_i \left[\frac{\partial \mathbf{U}}{\partial t} + (\mathbf{U} \cdot \nabla)\, \mathbf{U} \right] &= \frac{1}{\mu_0} (\nabla \times \mathbf{B}) \times \mathbf{B} - \nabla P && (4.15)\\ \frac{P}{n^\gamma} &= \text{const.} && (4.16) \end{aligned}$$

Following the steps of Section 4.1, the resulting dispersion relation of the ion-acoustic wave is given by

$$\left(\frac{\omega}{k}\right)^2 = \frac{\gamma p_0}{n_0 m_\mathrm{i}} \equiv c_s^2, \tag{4.17}$$

where the ion-sound speed c_s was introduced.

4.3 Generalised MHD modes

The system of equations (3.22), (3.23) and (3.24), an isotropic equation of state (3.20) and the Maxwell's equations (3.10), (3.11) and (3.12) comprise a closed system. This system is linearised by the scheme

$$\begin{aligned} n &= n_0 + \tilde{n}_1 && (4.18)\\ P &= P_0 + \tilde{P}_1 && (4.19)\\ P_e &= P_{0\mathrm{e}} + \tilde{P}_{1\mathrm{e}} && (4.20)\\ \mathbf{U} &= \mathbf{0} + \tilde{\mathbf{U}}_1 && (4.21)\\ \mathbf{E} &= \mathbf{0} + \tilde{\mathbf{E}}_1 && (4.22)\\ \mathbf{B} &= \mathbf{B}_0 + \tilde{\mathbf{B}}_1, && (4.23) \end{aligned}$$

where the perturbations are assumed to be plane waves propagating along the x-axis at an angle α to the background magnetic field $\mathbf{B}_0 = B_0 (\cos\alpha, 0, \sin\alpha)$.

The system has a non-trivial solution only if the following dispersion relation holds

$$\begin{aligned}
&\left(1+\lambda_{\mathrm{e}}^2k^2\right)^2\omega^6\\
&-\left[k^2c_s^2\left(1+\lambda_{\mathrm{e}}^2k^2\right)^2+k^2V_A^2\left(1+\lambda_{\mathrm{e}}^2k^2\right)+k^2V_A^2\cos^2\alpha\left(1+\lambda_{\mathrm{e}}^2k^2\right)\right]\omega^4\\
&+\left[2k^4V_A^2c_s^2\cos^2\alpha\left(1+\lambda_{\mathrm{e}}^2k^2\right)+k^4V_A^4\cos^2\alpha\right]\omega^2-k^6V_A^4c_s^2\cos^4\alpha\\
&=\lambda_{\mathrm{i}}^2k^4V_A^2\cos^2\alpha\left(\omega^2-k^2c_s^2\right)\omega^2, \qquad (4.24)
\end{aligned}$$

where the inertial lengths $\lambda_{\mathrm{e,i}}$, the Alfvén speed V_A and the ion-sound speed c_s given by (2.7), (4.9) and (4.17), were introduced. Regarding the correction due to electron inertia in the form of the factor $\left(1+\lambda_{\mathrm{e}}^2k^2\right)$, a typical ionospheric F region value of λ_{e}, adapted from Paper IV, is ~ 10m. Thus, for wavelengths larger than 1 km, the term $\lambda_{\mathrm{e}}^2k^2$ is less than 1%. Electron-inertial effects have been neglected in all included papers except for II and IV.

Neglecting electron intertia ($\lambda_{\mathrm{e}}=0$) in Eq. (4.24) gives the dispersion relation

$$\begin{aligned}
&\left(\omega^2-k^2V_A^2\cos^2\alpha\right)\left[\omega^4-k^2\left(V_A^2+c_s^2\right)\omega^2+k^4V_A^2c_s^2\cos^2\alpha\right]\\
&=\lambda_{\mathrm{i}}^2k^4V_A^2\cos^2\alpha\left(\omega^2-k^2c_s^2\right)\omega^2. \qquad (4.25)
\end{aligned}$$

Setting $\lambda_{\mathrm{i}}=0$ gives the ideal MHD modes

$$\omega^2 = k^2V_A^2\cos^2\alpha \qquad (4.26)$$

$$\omega^2 = k^2\frac{\left(V_A^2+c_s^2\right)\pm\sqrt{\left(V_A^2+c_s^2\right)^2-4V_A^2c_s^2\cos^2\alpha}}{2}, \qquad (4.27)$$

where the former is the Alfvén (shear, torsional, or slow) mode, which is incompressible and is associated with magnetic field perturbations only orthogonally to $\mathbf{B}_0$, in analogy to the twisting and plucking of a guitar string. This wave mode was first derived by Alfvén (1942). The latter constitutes two compressional modes, the fast and slow magnetosonic modes, given by the plus and minus signs, respectively. These modes resemble a sound wave and involve compression and rarefaction of $\mathbf{B}_0$. Their dispersion relation has the following limits

$$\left.\begin{array}{ll}\omega^2= & k^2V_A^2\\ \text{or} & \\ \omega^2= & k^2c_s^2\end{array}\right\}\ \text{if } \alpha=0 \qquad (4.28)$$

and

$$\left.\begin{array}{ll}\omega^2= & k^2\left(V_A^2+c_s^2\right)\\ \text{or} & \\ \omega^2= & 0\end{array}\right\}\ \text{if } \alpha=\pi/2. \qquad (4.29)$$

In the case of parallel propagation, the ion-sound and Alfvén modes decouple, whereas in perpendicular propagation the dispersion relation reduces to one magnetosonic mode.

4.3.1 Whistlers and drift waves

Returning now to equation (4.25), the implication of the term related to ion-inertial length on the right hand side is most easily realised by studying the generalised Ohm's law in the limit of neglected electron inertia and electron pressure gradients. Assuming stationary ions, (3.24) can be written

$$\frac{\partial \mathbf{B}}{\partial t} = -\frac{1}{ne}\nabla \times (\mathbf{J} \times \mathbf{B}) - \nabla \left(\frac{1}{ne}\right) \times (\mathbf{J} \times \mathbf{B}), \tag{4.30}$$

where, as we will see, the first (second) term in the right hand side gives rise to a whistler (drift) wave mode.

Linearising Eq. (3.24) with

$$n = n_0 + \tilde{n}_1 \tag{4.31}$$
$$\mathbf{B} = B_0\hat{\mathbf{z}} + \tilde{\mathbf{B}}_1, \tag{4.32}$$

where the perturbations are assumed to be plane waves propagating along the z-axis, (4.30) gives (e.g. Hassam and Huba, 1988)

$$\omega^2 = k^4 V_A^2 \lambda_\mathrm{i}^2, \tag{4.33}$$

which is the dispersion relation for whistler waves in the limit $1/k \ll \lambda_\mathrm{i}$.

Now we allow a background density gradient, linearise (4.30) with

$$n = n_0(x) + \tilde{n}_1 \tag{4.34}$$
$$\mathbf{B} = B_0\hat{\mathbf{z}} + \tilde{\mathbf{B}}_1 \tag{4.35}$$

and assume plane wave perturbations along the y-axis. We then obtain a dispersion relation for a magnetic drift wave mode (e.g. Hassam and Huba, 1987; Huba, 1991)

$$\omega = kV_A \frac{\lambda_\mathrm{i}}{L_n}, \tag{4.36}$$

where the density gradient scale $L_n = (\partial \ln n_0/\partial x)^{-1}$ has been assumed to obey $L_n \ll \lambda_\mathrm{i}$. The magnetic drift mode is, in contrast to the whistler mode, non-dispersive and propagates in the direction $\mathbf{B}_0 \times \nabla n_0$.

4.4 The stationary wave frame

We wish to study the behaviour of the plasma waves described by (4.25) in their own frame of reference. Assuming a wave propagating with velocity $\mathbf{W} = W\hat{\mathbf{x}}$ in the laboratory frame of reference and allowing gradients only in the $\hat{\mathbf{x}}$-direction, the stationary wave frame equations are derived by the substitutions

$$x \mapsto x' + Wt \tag{4.37}$$
$$t \mapsto t' \tag{4.38}$$
$$\frac{\partial}{\partial x} \mapsto \frac{\partial}{\partial x'} \tag{4.39}$$
$$\frac{\partial}{\partial t} \mapsto -W\frac{\partial}{\partial x'}, \tag{4.40}$$

where primed quantities are measured in the wave frame of reference. The electric, magnetic and velocity fields are given by their non-relativistic Lorentz transformations (Jackson, 1999)

$$\mathbf{E} \mapsto \mathbf{E}' - \mathbf{W} \times \mathbf{B} \tag{4.41}$$
$$\mathbf{B} \mapsto \mathbf{B}' \tag{4.42}$$
$$\mathbf{U} \mapsto \mathbf{U}' + \mathbf{W}. \tag{4.43}$$

This scheme is applied on (3.20), (3.22)-(3.24) and (3.10)-(3.12), where electron inertia and electron pressure gradients are neglected. Linearising in the same manner as in Section 4.3 and assuming perturbations $\propto e^{Kx}$, gives the dispersion relation (Stasiewicz, 2004, 2005)

$$\lambda_{\mathrm{i}}^2 K^2 = \frac{\left(M^2 - \cos^2\alpha\right)^2}{M^2\cos^2\alpha}\left[\frac{2M^2\sin^2\alpha}{\left(2M^2 - \gamma\beta\right)\left(M^2 - \cos^2\alpha\right)} - 1\right], \tag{4.44}$$

where $M = -\frac{U'_{x0}}{V_A}$ is the Machnumber, U'_{x0} is the background plasma flow in the frame of reference of the wave and β is defined in (2.6). (4.44) is equivalent to (4.25) through the substitutions $M \mapsto \frac{\omega/k}{V_A}$, $K \mapsto \mathrm{i}k$ and $\gamma\beta \mapsto \frac{2c_s^2}{V_A^2}$.

It is seen that the two roots $K_{1,2} = \pm\sqrt{K^2}$ of (4.44) are either purely imaginary or real. $K^2 < 0$ corresponds to sinusoidal solutions, whereas $K^2 > 0$ describes exponentially-varying solitary waves. If one retains terms related to electron inertia in (3.24) (e.g. Paper I), the dispersion relation will be in the form $K^4R^2M^2 + K^2\cos^2\alpha\left(1 - C_1R\right) + C_2 = 0$, where $C_1, 2$ are constants. Such a dispersion relation enables $K \in \mathbb{C}$ with simultaneously non-zero real and imaginary parts. Such waves with oscillatory amplitudes have been identified in multi-ion plasmas and are called oscillitons (Sauer et al., 2001, 2003; Dubinin et al., 2003).

We now examine the regions of the phase space spanned by M and $\cos\alpha$ where (4.44) admits solitary wave solutions by plotting only $\lambda_{\mathrm{i}}^2 K^2 > 0$. Figure 4.1 shows an example for $\beta = 10^{-5}$ and $\gamma = 5/3$, applicable for the Earth's ionospheric F

region. The coloured regions describe the parameter space where exponentially growing solitary wave solutions are allowed. The remaining regions are subject to sinusoidal waves.

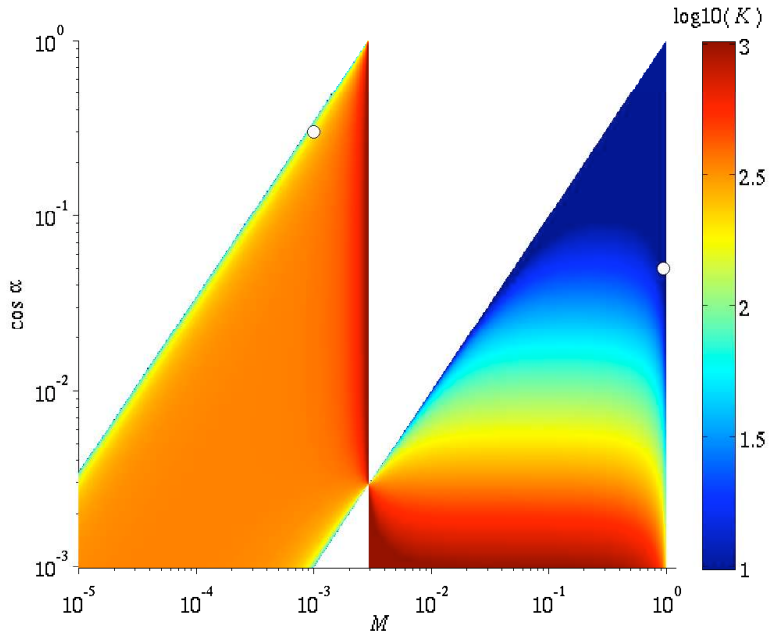

Figure 4.1. Spatial growth rate K (normalised to $1/\lambda_i$), (4.44), for solitary waves propagating at an angle α to $\mathbf{B}_0$ with the Mach number $M = \frac{\omega}{kV_A}$ in an isotropic plasma with $\beta = 10^{-5}$ $\gamma = 5/3$. The black-edged white circles indicate the M- and $\cos\alpha$-values for which wave solutions are shown in Figure 4.2.

The linear MHD modes corresponding to the limit $K \to 0$ of (4.44) are found along the edges of the surfaces in Figure 4.1. The left (right) surface is bounded by the slow (fast) magnetosonic mode, next to the white circle, the vertical boundary in the form of the sonic shock line and the shear Alfvén mode. The sonic shock line corresponds to $M = \sqrt{\gamma\beta/2} = c_s/V_A$, which separates slow modes from fast modes. The sonic shock line and the shear Alfvén mode intersect at the sonic shock angle (Stasiewicz, 2005) $\alpha_s = \arccos\sqrt{\gamma\beta/2}$, which separates Alfvén modes propagating subsonically and supersonically. Consequently, in low-β plasmas, the subsonic modes will only propagate at close to perpendicular angles.

Figure 4.2 shows two examples of solitary wave solutions corresponding to the plasma environment defined by Figure 4.1. The blue (red dashed) curve describes normalised plasma density associated with a solitary wave train propagating along the x-axis at 73° (87°) angle to the background magnetic field with the

Mach number $M = 1.0 \times 10^{-3}$ ($M = 0.95$). The M and $\cos\alpha$ values are shown as black-edged white circles in Figure 4.1. Solitary wave solutions corresponding to the left (right) region of Figure 4.1 form compressive (rarefactive) structures with an associated positive (negative) electric potential (e.g. Paper I).

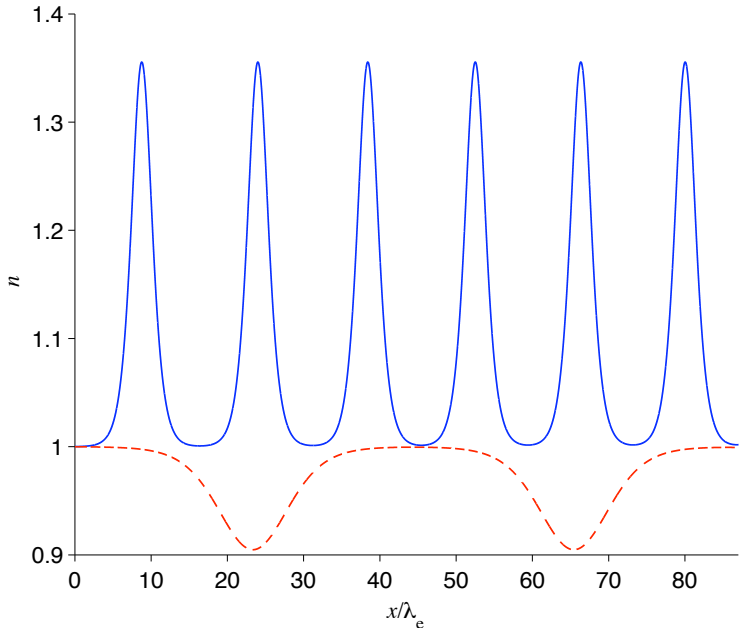

Figure 4.2. The blue (red dashed) curve shows normalized plasma density associated with a solitary wave train propagating along the x-axis at 73° (87°) angle to the background magnetic field with the Mach number $M = 1.0 \times 10^{-3}$ ($M = 0.95$). The x-axis is normalized to the electron inertial length, λ_e, and the spatial extent of the rarefactive structure (red dashed curve) has been scaled down by a factor 10. The structures propagate in a plasma defined by Figure 4.1.

CHAPTER 5

The Ionosphere

This chapter will give a brief introduction to the Earth's ionosphere, but in doing so it is useful to first state some basic characteristics of the atmosphere. Both the atmosphere and the ionosphere are essentially stratified. The atmospheric layers are related to an altitude profile of temperature, where the vertical gradient changes sign in every layer. The ionospheric layers, on the other hand, are better described by an altitude profile of the electron number density.

The left panel of Figure 5.1 shows the altitude profile of temperature in the atmospheric layers. Starting from below, the *troposphere* is a turbulent layer where most of the phenomena related to our everyday weather takes place. The temperature falls with height up to about 12 km altitude, where the tropopause is located. The tropopause, which is a temperature inversion layer, separates the troposphere from the *stratosphere*. The latter is associated with a temperature increase with height primarily due to UV* absorption by ozone leading to a local temperature maximum at the stratopause. The next layer is the *mesosphere*, where radiative cooling creates a sharp temperature decrease to a minimum in the range $130 - 190$ K (Kelley, 1989) at the mesopause. Ascending further, the temperature in the *thermosphere* increases dramatically to a value often well above 1000 K and then remains nearly constant with height. The lowest 100 km of the atmosphere constitutes the *homosphere*, which is relatively uniform in composition due to turbulent mixing. In the *heterosphere*, on the other hand, air is poorly mixed due to the low molecular collision frequency.

The concept of an electrically charged region in the upper atmosphere dates back to the instrument maker George Graham in London who in 1722 observed daily variations of the Earth's magnetic field and irregular magnetic disturbances later attributed to magnetic storms. In the context of the latter, he introduced the distinction between magnetically *quiet* and *disturbed* days (Evans, 1975; Courtillot and Le Mouel, 1988). Gauss (1838) suggested that these magnetic disturbances were induced by currents flowing in the atmosphere, an idea which was further

*Ultraviolet radiation is the part of the electromagnetic spectrum with wavelengths 10 – 400 nm.

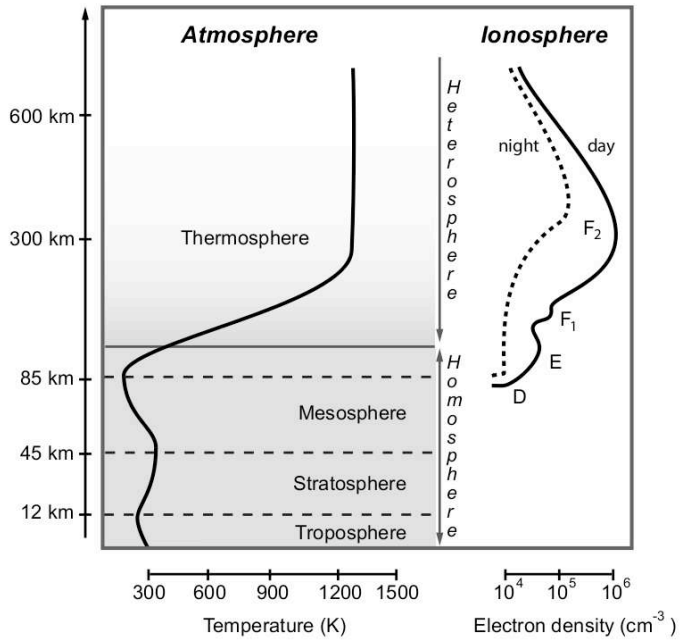

Figure 5.1. Schematic picture of the atmospheric (left) and ionospheric (right) layers (After Engwall, 2009, with kind permission from E. Engwall).

developed by Stewart (1882).

After Marconi's demonstration of trans-Atlantic radio communication in 1901 (Marconi, 1902a,b,c), Kennelly (1902) and Heaviside (1902) independently assessed the idea of an ionised layer as a means of bending radio waves around the curved Earth. Their ideas were later confirmed by Appleton and Barnett (1926), who demonstrated the existence of the so-called *Kennelly-Heaviside layer*, also known as the E layer or E region.

5.1 Formation of the ionosphere

Photons from the sun, essentially in the UV range, impinging on the Earth's atmosphere create an ionised component through reactions of the type

$$X + h\nu \rightarrow X^+ + e^-, \tag{5.1}$$

where X is a neutral atmospheric component, such as O (oxygen) and NO (nitric oxide). Another source of ionisation, particularly important at high latitudes, is the flux of electrons during auroras and energetic protons produced by solar

Table 5.1. Altitude range, representable electron density, n_e and dominant ion species for the respective ionospheric regions (Kelley, 1989; Fälthammar, 1999).

Layer	D	E	F_1	F_2
Altitude range [km]	60–90	90–150	150–200	200–1500
Daytime n_e [10^{10} m^{-3}]	0.1	10–20	20–50	50–200
Nighttime n_e [10^{10} m^{-3}]	<0.01	0.2	–	20–50
Ion species	NO^+, O_2^+	NO^+, O_2^+	O^+	O^+
			NO^+, O_2^+	H^+, He^+

flares. The ionised component is reduced through dissociative and radiative recombination exemplified respectively by

$$NO^+ + e^- \rightarrow N + O \tag{5.2}$$

and

$$O^+ + e^- \rightarrow O + h\nu. \tag{5.3}$$

At altitudes where collisions are infrequent, the recombination rate is slow and consequently a permanent population of ionised atmosphere, the *ionosphere*, is formed. The Earth's ionosphere begins around 60 km altitude and without a clear border to the magnetosphere it extends to an altitude of more than 1000 km. Three factors determine the electron density at a certain height; the atmospheric neutral density, the intensity of the ionising radiation and the ion recombination rate. The atmospheric density decreases with height, the radiation intensity increases and the recombination rate varies significantly between different ion species. For instance, NO^+ recombines nearly 1000 times faster than O^+ and consequently molecular ions are much more short-lived than atomic ions. Also, the atmospheric neutral constitution is altitude-dependent. Consequently, several ionospheric layers with a pronounced electron density, similar to the Kennelly-Heaviside layer, will form. The right panel of Figure 5.1 provides a schematic picture of these layers and Table 5.1 summarises the corresponding altitude ranges, the day- and nighttime electron densities and the dominating ion species number densities in descending order (Kelley, 1989; Fälthammar, 1999).

We see that the F region, or *Appleton layer*, contains the global maximum in electron density in the ionosphere. At altitudes above the peak, a decreasing neutral density lowers the ionisation rate, and below the peak, the intensity of the

ionising radiation decreases. The region consists of two local electron density maxima, the $F1$ and $F2$ peaks, where the former vanishes during nighttime. The ionospheric F region peak mentioned in Papers IV, V and VI refers to the $F2$ peak.

The ionospheric layers all play an important role in radio wave propagation. LF-, MF- and HF[†] radio waves are reflected mainly from respectively the D-, E-, and F layers. Thus, higher frequences are reflected at higher electron densities. It turns out that an ionospheric layer with plasma frequency ω_{pe} always will reflect waves with frequency $\omega \leq \omega_{pe}$, whereas waves with frequency $\omega > \omega_{pe}$ are reflected only if $\omega < \omega_{\rm pe}/\cos\alpha$, where α is the angle between the propagation direction of the wave and the vertical. That is, higher frequences can only be reflected if they propagate at a sufficiently large angle to the vertical, otherwise they will penetrate through the layer (Budden, 1985).

[†]Low Frequency, Medium Frequency and High Frequency refers to radio frequencies in the respective ranges 30 kHz – 300 kHz, 300 kHz – 3 MHz and 3 MHz – 30 MHz.

CHAPTER 6

Scattering of radio waves from an ionospheric plasma

As was shown in Chapter 5, the ionosphere contains enough charged particles to cause measurable effects on the propagation of radio waves. Incoherent scatter radars utilise this effect and are a means of probing the ionospheric plasma to extract information on the plasma density, ion- and electron temperatures and line-of-sight ion velocity. It will be shown later in this chapter that the radar scattering is intimately linked to three wave modes described by two-fluid theory, which was introduced in Section 3.2. We therefore start off by introducing these waves and will later return to the incoherent scatter technique and discuss the associated spectra.

6.1 Unmagnetised plasma waves in two-fluid theory

We wish to study waves in a plasma without a background magnetic field, or equivalently, waves in a plasma where all motions are parallel to the background magnetic field. The two-fluid equation of motion is repeated from (3.19) and the electric field is expressed as

$$n_\alpha m_\alpha \left[\frac{\partial \mathbf{u}_\alpha}{\partial t} + (\mathbf{u}_\alpha \cdot \nabla)\,\mathbf{u}_\alpha\right] = q_\alpha n_\alpha (\mathbf{E} + \mathbf{u}_\alpha \times \mathbf{B}) - \nabla P_\alpha \tag{6.1}$$

$$\mathbf{E} = -\nabla\Phi - \frac{\partial \mathbf{A}}{\partial t}, \tag{6.2}$$

where the vector potential $\mathbf{A}$ satisfies $\mathbf{B} = \nabla \times \mathbf{A}$ and we choose the Coulumb gauge (Jackson, 1999) $\nabla \cdot \mathbf{A} = 0$.

We shall distinguish between electrostatic and electromagnetic waves through the treatment of the momentum equation. The former are derived by studying the divergence of (6.1), whereas the latter originate from a curl of (6.1). Consequently, the electrostatic waves are associated with perturbations along the electric field

and a finite pressure, whereas the electromagnetic waves involve transverse perturbations and zero pressure. The linearisation scheme in both cases is given by

$$\begin{aligned} n_\alpha &= n_{\alpha 0} + \tilde{n}_{\alpha 1} && (6.3)\\ \mathbf{u}_\alpha &= \mathbf{0} + \tilde{\mathbf{u}}_{\alpha 1} && (6.4)\\ P_\alpha &= P_{\alpha 0} + \tilde{P}_{\alpha 1} && (6.5)\\ \mathbf{E} &= \mathbf{0} + \tilde{\mathbf{E}}_1 && (6.6)\\ \mathbf{B} &= \mathbf{0} + \tilde{\mathbf{B}}_1. && (6.7) \end{aligned}$$

6.1.1 Electrostatic waves

In addition to (6.1) and (6.2), we utilise the continuity equation (3.18), an equation of state (3.20) and Gauss' law (3.9):

$$\begin{aligned} \frac{\partial n_\alpha}{\partial t} + \nabla \cdot (n_\alpha \mathbf{u}_\alpha) &= 0 && (6.8)\\ P_\alpha &\propto n_\alpha^{\gamma_\alpha} && (6.9)\\ \nabla \cdot \mathbf{E} &= \rho/\varepsilon_0. && (6.10) \end{aligned}$$

Linearising this system of equations, while utilising the divergence of (6.1), and assuming perturbations in the form of plane waves, gives the dispersion relation

$$1 + \sum_\alpha -\omega_{p\alpha}^2 \left(\omega^2 - \frac{\gamma_\alpha P_{\alpha 0} k^2}{m_\alpha n_{\alpha 0}} \right)^{-1} = 0, \tag{6.11}$$

where the plasma was assumed to be initially charge neutral. Now, assuming the species to obey the ideal gas law, $P_{\alpha 0} = n_{\alpha 0} k_\mathrm{B} T_{\alpha 0}$, the above dispersion relation turns into

$$1 + \sum_\alpha \chi_\alpha = 0, \tag{6.12}$$

where

$$\chi_\alpha = -\frac{\omega_{p\alpha}^2}{\omega^2 - k^2 \gamma_\alpha k_\mathrm{B} T_{\alpha 0}/m_\alpha} \tag{6.13}$$

is the susceptibility of species α. Two obvious limits to (6.13) exist, namely $\omega/k \gg v_{\mathrm{th},\alpha}$ and $\omega/k \ll v_{\mathrm{th},\alpha}$, where $v_{\mathrm{th},\alpha} = \sqrt{2 k_B T_{\alpha 0}/m_\alpha}$ is the thermal (most probable) speed of species α. The former limit is adiabatic with γ_α given by (3.21). Because the plane wave perturbations are unidirectional, the associated compression will have only one degree of freedom, thus $\gamma_\alpha = 3$. The latter limit is isothermal with $\gamma_\alpha = 1$.

In a plasma consisting of electrons and one type of ions, three situations, based on the adiabatic and the isothermal limits, can occur. Either both electrons and ions

are isothermal, both electrons and ions are adiabatic, or the electrons are isothermal and the ions are adiabatic. The fully isothermal situation corresponds to the Debye shielding introduced in Section 2.1, while the fully adiabatic situation leads to (Bellan, 2006)

$$\omega^2 = \omega_{p\mathrm{e}}^2 + 3k^2\frac{k_\mathrm{B}T_{\mathrm{e}0}}{m_\mathrm{e}}, \tag{6.14}$$

known as the *electron plasma wave*, the *Langmuir wave* (Langmuir, 1928), or the *Bohm-Gross wave* (Bohm and Gross, 1949). The mixed situation with adiabatic ions and isothermal electrons corresponds to *ion-acoustic waves*, which are described by (Bellan, 2006)

$$\omega^2 = k^2\frac{\Lambda_{D\mathrm{e}}^2\omega_{p\mathrm{i}}^2}{1+k^2\Lambda_{D\mathrm{e}}^2} + 3k^2\frac{k_\mathrm{B}T_{\mathrm{i}0}}{m_\mathrm{i}}. \tag{6.15}$$

It can be seen from (6.15) that in order to fulfill the assumption of adiabatic ions, the right hand side must be dominated by the first term. That is, ion-acoustic waves can only propagate if $T_\mathrm{e} \gg T_\mathrm{i}$ and will otherwise be strongly attenuated, a concept known as Landau damping. Note that the MHD ion-sound dispersion relation, (4.17), is retained in the limit of long wavelengths $k^2\Lambda_{D\mathrm{e}}^2 \ll 1$.

6.1.2 Electromagnetic waves

This time, (6.1) and (6.2), are supplemented by Ampère's law (3.12) and the definition of current density (3.16);

$$\nabla\times\mathbf{B} = \mu_0\mathbf{J} + \varepsilon_0\mu_0\frac{\partial\mathbf{E}}{\partial t} \tag{6.16}$$

$$\mathbf{J} = \sum_\alpha q_\alpha n_\alpha \mathbf{u}_\alpha. \tag{6.17}$$

Linearising this system, while utilising the curl of (6.1) and assuming plane wave perturbations, gives the dispersion relation for an electromagnetic wave in an unmagnetised plasma:

$$\omega^2 = \omega_p^2 + k^2c^2, \tag{6.18}$$

where $\omega_p = \sum_\alpha \omega_{p\alpha}$ is the total plasma frequency. In the limit of no plasma, the standard vacuum electromagnetic wave is retained. It is also seen that for $\omega < \omega_p$, $k^2 < 0$ and hence the wave does not propagate, in accordance with the discussion in the last paragraph of Section 5.1.

6.2 Incoherent scatter theory

The theory of scattering of radio waves off randomly distributed electrons in the ionosphere was first outlined in the late 1950's by Gordon (1958), who suggested this ground-based method as a means of estimating the electron density and temperature in the ionosphere. Soon after that, Bowles (1958) conducted the first observation and found that the frequency spectrum was associated with the ion temperature rather than the electron temperature. He also estimated a much lower electron density than expected. Kahn (1959) later shed light on the previous observations by showing that the scattering cross-section[‡] was affected by the Coulomb interaction between the electrons and ions and that the scattering was not a fully random process.

Returning to the concept of Debye length introduced in Section 2.1, it turns out that the scattering is qualitatively dependent on how the wavelength of the scattered radiation compares to the Debye length. At this point it is convenient to introduce the dimensionless parameter α according to (Bauer, 1975)

$$\alpha = \frac{1}{k\Lambda_{D\mathrm{e}}}, \tag{6.19}$$

where k is the magnitude of $\mathbf{k} = \mathbf{k}_s - \mathbf{k}_i$ as defined by the geometry in Figure 6.1. The figure describes how an incoming electromagnetic wave with wave vector $\mathbf{k}_i$ and frequency ω_i impinges on a particle and is scattered to $\mathbf{k}_s, \omega_s$ at the scattering angle θ to $\mathbf{k}_i$. It can be shown (e.g. Sheffield, 1975) that the scattered power from a freely moving charge is inversely proportional to the square of the mass of the charge. Scattering from ions can therefore be neglected in comparison to that from the electrons. Consequently, the relevant scale of the shielding is the electron Debye length, rather than the total Debye length (see Section 2.1).

We see from (6.19) that an electromagnetic wave with wavelength $\lambda = 2\pi/k \ll \Lambda_{D\mathrm{e}}$ corresponds to $\alpha \ll 1$. In a plasma in thermodynamic equilibrium, such a wave would experience the plasma on a scale where all charges appear to be free. The limit of $\alpha \ll 1$ describes incoherent scattering or non-collective scattering and the spectrum reflects the electron velocity distribution. This is the result that Bowles (1958) had expected to get in his first experiment mentioned above. However, when the wavelength is larger than the Debye length and $\alpha \geq 1$, shielding effects become important. The incident wave will now scatter from the electrons shielding ions and other electrons. Consequently, not only the electrons but also the ion movements will affect the shape of the spectrum.

We put these limits in an observational context by calculating $\Lambda_{D\mathrm{e}}$ for the ionospheric parameters given in Paper IV and compare with the probing wavelength of the European Incoherent Scatter Svalbard Radar (Wannberg et al., 1997), which has been utilised in Papers IV,V and VI. The Debye length is found to be 0.7 cm

[‡]The scattering cross-section is a hypothetical area describing the probability of radiation being scattered by a particle.

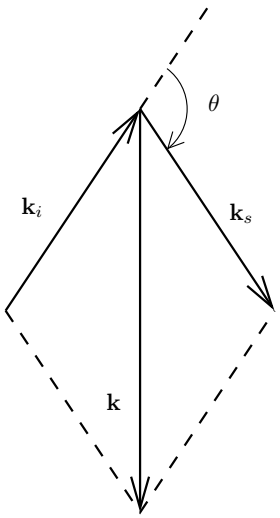

Figure 6.1. Geometry of an incident (scattered) electromagnetic wave with wave vector $\mathbf{k}_i$ ($\mathbf{k}_s$) impinging on a particle and being scattered by the angle θ.

and the radar wavelength is 0.6 m. Thus, the scattering is far from purely incoherent and in fact, the spectrum from an incoherent scatter radar always contains a coherent component.

6.2.1 Calculating the spectrum

The scattering cross-section, and hence the scattered spectrum, is determined by the spectral density of electron-density fluctuations. These fluctuations were described independently by Dougherty and Farley (1960), Fejer (1960), Renau (1960) and Salpeter (1960), assuming a stationary, uniform, unmagnetised and collisionless plasma in thermodynamic equilibrium. The last condition was somewhat relaxed in the treatment of Salpeter (1960), who allowed small departures from equilibrium due to unequal electron and ion temperatures and multiply charged ions. Hagfors (1960) included a constant magnetic field into the calculations. Using a method of dressed test particles (Rostoker, 1964a), Rosenbluth and Rostoker (1962), Rostoker (1964b) and Rostoker (1964c) extended the theory to allow for large departures from thermal equilibrium in magnetised plasmas. A theory of thermal fluctuations for a non-uniform and non-stationary plasma was developed by Weinstock (1965, 1967).

For our purposes it is sufficient to consider the approach of Salpeter (1960), i.e. allowing for small departures from thermodynamic equilibrium through unequal electron and ion temperatures in an unmagnetised, collisionless and non-relativistic plasma ($v/c \ll 1$). The assumption of an unmagnetised plasma is

equivalent to only considering motions along the magnetic field, as utilised in Section 6.1, and which is the case in the radar-oriented Papers IV, V and VI, where the radar's line-of-sight is parallel to the geomagnetic field. We further assume a scattering volume $V = L^3$ with on average N electrons and N/Z ions of charge Ze such that $L, 2\pi/k_i \ll |\mathbf{R}|$, where $\mathbf{R}$ is the location of the observer relative to the scattering volume. Finally, we assume an incident wave frequency $\omega_i > \omega_{pe}$ and a scattering volume small enough to prevent multiple scattering and to transmit the wave without considerable damping. The average scattered power in the frequency range $[\omega_s, \omega_s + \mathrm{d}\omega_s]$ into the solid angle $\mathrm{d}\Omega$ observed at $\mathbf{R}$ is then given by (Sheffield, 1975)

$$P_s(\mathbf{R}, \omega_s)\mathrm{d}\Omega\mathrm{d}\omega_s = \frac{P_i r_0^2}{2\pi} n_e L \left|\hat{\mathbf{k}}_s \times \left(\hat{\mathbf{k}}_s \times \hat{\mathbf{p}}\right)\right|^2 S(\mathbf{k}, \omega)\mathrm{d}\Omega\mathrm{d}\omega_s, \tag{6.20}$$

where $\hat{\mathbf{p}}$ is the unit polarisation vector, $r_0 = e^2/(4\pi\varepsilon_0 m_\mathrm{e} c^2)$ is the classical electron radius and

$$S(\mathbf{k}, \omega) = \frac{2\pi}{k}\left|1 - \frac{\chi_\mathrm{e}}{\epsilon}\right|^2 f_{\mathrm{e}0}\left(\omega/k\right) + \frac{2\pi Z}{k}\left|\frac{\chi_\mathrm{e}}{\epsilon}\right|^2 f_{\mathrm{i}0}\left(\omega/k\right) \tag{6.21}$$

is the spectral density function. $f_{\alpha 0}$ denotes the inital velocity distributions. χ_α, the susceptibility of species α (e, i), and ϵ, the longitudinal dielectric function, are defined by

$$\chi_\alpha(\mathbf{k}, \omega) = \frac{\omega_{p\alpha}^2}{k^2} \lim_{\gamma \to 0} \int_{-\infty}^{+\infty} \frac{\mathbf{k} \cdot \partial f_{\alpha 0}/\partial \mathbf{v}}{\omega - \mathbf{k} \cdot \mathbf{v} - i\gamma} \mathrm{d}\mathbf{v} \tag{6.22}$$

$$\epsilon(\mathbf{k}, \omega) = 1 + \chi_\mathrm{e}(\mathbf{k}, \omega) + \chi_\mathrm{i}(\mathbf{k}, \omega). \tag{6.23}$$

It can be seen from (6.20) that the spectral behaviour of the scattered power is fully contained in S, which is also called the *form factor* (Froula et al., 2011) since it defines the qualitative shape of the spectrum. The first (second) term in (6.21) represents the electron (ion) component.

The susceptibilities defined in (6.22) are proportional to $\alpha^2 = (k\Lambda_{D\mathrm{e}})^{-2}$ and in the incoherent scatter limit $\alpha \to 0$ the spectral behaviour of S is fully contained in the electron distribution function. The remaining part of the electron component and the ion component contains the shielding of electrons and ions, respectively. These terms become particularly important when $\alpha \gtrsim 1$ and $|\epsilon|$ is small at the natural resonances of the plasma. In an unmagnetised plasma these resonances occur at the frequences of the electron plasma and the ion-acoustic waves defined respectively by (6.14) and (6.15), thus close to the plasma and ion-acoustic frequencies.

Figure 6.2 shows a theoretical incoherent scatter spectrum based on (6.21) as seen by a 500 MHz radar observing a plasma characterised by $T_\mathrm{i} = 1000$ K, $T_\mathrm{e}/T_\mathrm{i} = 2$, $m_\mathrm{i} = 16$ u, $n_\mathrm{e} = 1.0 \times 10^{11}$ m^{-3} and no ion-drifts. Only positive frequencies are shown, but a spectrum from a thermal plasma is symmetrical around the

zero-frequency if there are no drifts present along the radar beam. The broad feature close to zero-frequency constitutes half of the ion line and the narrow high-frequency feature is one of the plasma lines. The ion line really consists of two separate lines formed by scattering of the incident signal off ion-acoustic waves, but due to Landau damping, the lines are broadened and merge into a "double-humped" line with a downshifted and an upshifted shoulder, corresponding to scattering off ion-acoustic waves propagating respectively away from and towards the radar. The plasma lines are formed by scattering off Langmuir waves and the power contained in these lines is much less than in the ion line simply because there are fewer electrons matching the Langmuir phase velocity than the ion-acoustic phase velocity. The spectra addressed hereafter and those contained in Papers IV, V and VI all refer to the ion line component of the incoherent scatter spectra. As was noted already by Bowles (1958), the incoherent scatter spectrum

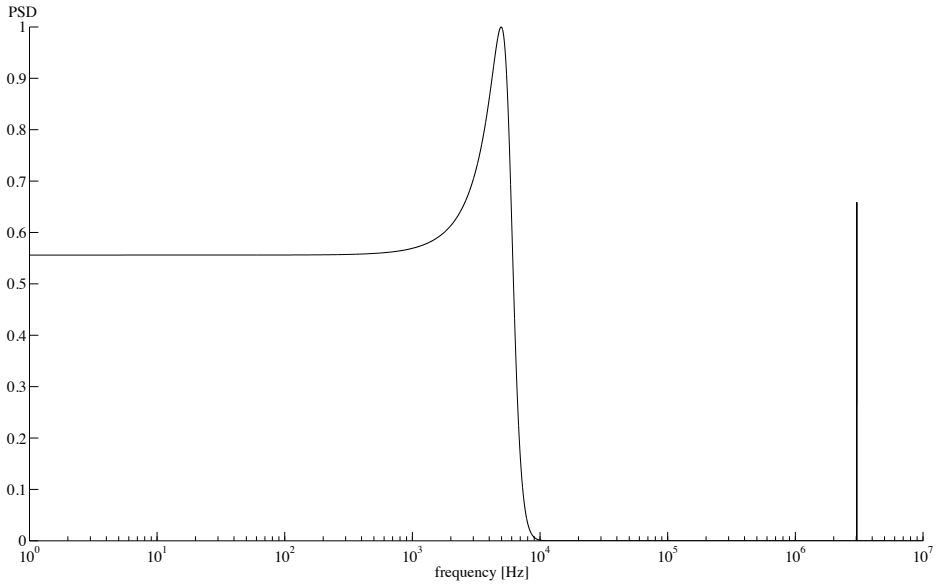

Figure 6.2. Theoretical incoherent scatter spectrum based on (6.21) for a 500 MHz incoherent scatter radar. The x axis shows frequency and the y axis shows power spectral density in arbitrary units. Unless otherwise specified, the plasma is characterised by $T_\mathrm{i} = 1000$ K, $T_\mathrm{e}/T_\mathrm{i} = 2$, $m_\mathrm{i} = 16$ u, $n_\mathrm{e} = 1.0 \times 10^{11}$ m^{-3} and no ion-drifts.

contains information, not only about the electrons, but also about the ions. This collective part of the spectrum is to a large extent contained in the ion line. Figure 6.3 shows theoretical ion line spectra (< 20 kHz) for various plasmas as observed by a 500 MHz incoherent scatter radar. Unless otherwise specified, the plasma is characterised by $T_\mathrm{i} = 1000$ K, $T_\mathrm{e}/T_\mathrm{i} = 1$, $m_\mathrm{i} = 16$ u, $n_\mathrm{e} = 1.0 \times 10^{11}$ m^{-3} and $v_\mathrm{i} = 0$

m/s (ion velocity along the radar line-of-sight, positive away from the observer).

The top left panel of Figure 6.3 shows the dependence on T_i and m_i. It can be seen that the shoulders increase their separation with increasing T_i and decreasing m_i. It is also apparent from the ion lines corresponding to $\{T_\mathrm{i} = 1000$ K, $m_\mathrm{i} = 16$ u$\}$ and $\{T_\mathrm{i} = 2000$ K, $m_\mathrm{i} = 32$ u$\}$ that it is actually the ratio $T_\mathrm{i}/m_\mathrm{i}$ that defines the spectral width. This can be realised from the ion-acoustic dispersion relation (6.15). In the long wavelength limit ($k^2\Lambda_{D\mathrm{e}}^2 \ll 1$) and assuming singly charged ions, it simplifies to

$$\omega^2 = k^2 \frac{k_\mathrm{B} T_\mathrm{i}}{m_\mathrm{i}} \left(T_\mathrm{e}/T_\mathrm{i} + 3\right). \tag{6.24}$$

Recalling from the scattering geometry in Figure 6.1, that $\mathbf{k} = \mathbf{k}_s - \mathbf{k}_i$ and assuming $|\mathbf{k}_s| = |\mathbf{k}_i|$, we have $k^2 = 4k_i^2 \sin^2(\theta/2)$ and consequently the frequencies of the ion-acoustic shoulders for a radar with wavelength λ_i are given by

$$f_{ia} = \pm \frac{2}{\lambda_i} \sqrt{\frac{k_\mathrm{B} T_\mathrm{i}}{m_\mathrm{i}} \left(T_\mathrm{e}/T_\mathrm{i} + 3\right)}, \tag{6.25}$$

assuming backscattering ($\theta = 180°$). Thus, an increase in the $T_\mathrm{i}/m_\mathrm{i}$ ratio as well as in the $T_\mathrm{e}/T_\mathrm{i}$ ratio increases the separation of the ion-acoustic shoulders.

An important side-result in the last paragraph is the Bragg condition $k^2 = 4k_i^2 \sin^2(\theta/2)$, which defines the spatial scale of density fluctuations that a particular radar will be sensitive to, or in other words, which spatial Fourier component the radar will select. In the case of a monostatic radar (backscattering), this scale will be half of the radar wavelength.

In the the top right panel of Figure 6.3 we see that an increasing $T_\mathrm{e}/T_\mathrm{i}$ ratio, besides shifting the shoulders as described above, also increases the ratio of the peaks to the spectral valley between them. This is because, as stated in Section 6.1.1, the Landau damping of ion-acoustic waves decreases with an increasing temperature ratio.

The bottom left panel shows the effect of varying the electron density. It seems the scattered power is proportional to the electron density. In fact, the total power in the ion line can be shown (Buneman, 1962) to obey

$$P_\mathrm{ionline} \propto \frac{n_\mathrm{e}}{\left(1 + k^2\Lambda_{D\mathrm{e}}^2\right)\left(1 + T_\mathrm{e}/T_\mathrm{i} + k^2\Lambda_{D\mathrm{e}}^2\right)}. \tag{6.26}$$

In the limit of long wavelengths the total scattered power is therefore proportional to $n_\mathrm{e}/\left(1 + T_\mathrm{e}/T_\mathrm{i}\right)$.

Finally, the bottom right panel shows the effect of an ion-drift along the radar beam with $v_i > 0$ corresponding to a drift away from the observer. The way this Doppler shift arises is explained below. The parameter pair $\{\omega, \mathbf{k}\}$ observed in a fixed frame are related to their equivalents in a primed frame moving with velocity $\mathbf{V}$ relative to the fixed frame through the relations

$$\mathbf{k} = \mathbf{k}' \tag{6.27}$$

$$\omega = \omega' + \mathbf{V} \cdot \mathbf{k}, \tag{6.28}$$

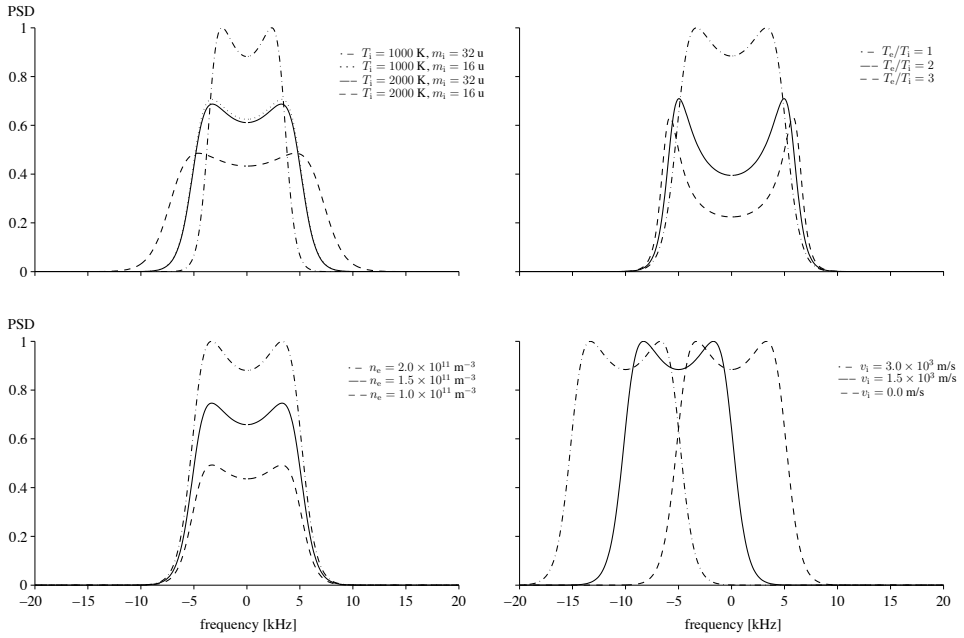

Figure 6.3. Theoretical ion line spectra based on (6.21) for a 500 MHz incoherent scatter radar. The x axes show frequency and the y axes show power spectral density in arbitrary units. The plasma is characterised by $T_\mathrm{i} = 1000$ K, $T_\mathrm{e}/T_\mathrm{i} = 1$, $m_\mathrm{i} = 16$ u, $n_\mathrm{e} = 1.0 \times 10^{11}$ m^{-3} and $v_\mathrm{i} = 0$ m/s (ion velocity along the radar line-of-sight, positive away from the observer), unless otherwise stated.

where the scattering takes place in the primed frame. If the ion-drift has a component along the radar beam directed away from (towards) the observer, the observed ion line spectrum will be shifted down (up) in frequency.

The plasma parameters mentioned above can be determined through an iterative fitting procedure while utilising Maxwellian spectra. This has been implemented in the EISCAT standard analysis software package GUISDAP (Lehtinen and Huuskonen, 1996). The plasma line can, in addition to the information from the ion line, supply yet another relation between electron density and electron temperature based on (6.14).

6.2.2 Enhanced ion lines

The fitting of plasma parameters from ion line measurements, as mentioned in the previous section, requires the plasma to be close to thermodynamic equilibrium. There are, however, phenomena that make the plasma unstable, and hence non-

Maxwellian, which results in a failing fitting procedure. There have been several studies on the effects that such non-Maxwellian ion velocity distributions have on the ion line spectrum (e.g. Raman et al., 1981; Kikuchi et al., 1989).

One example of plasma-destabilising phenomena is *naturally enhanced ion-acoustic lines* (NEIAL), a term which refers to spectral enhancements of one or both of the ion line shoulders sometimes observed when the radar beam is nearly parallel to the geomagnetic field. NEIAL were first observed by the Millstone Hill incoherent scatter radar (Foster et al., 1988) and have been seen with the European Incoherent Scatter (EISCAT) UHF (Rietveld et al., 1991), the EISCAT VHF (Collis et al., 1991) and the EISCAT Svalbard Radar (ESR) (Buchert et al., 1999). NEIAL are associated with spectral enhancements of up to 4–5 orders of magnitude above the thermal level (Grydeland et al., 2004), are often seen simultaneously over a height range of several 100 km (Rietveld et al., 1991) and have been observed up to 1900 km altitude (Ogawa et al., 2006).

NEIAL are associated with scattering off destabilised ion-acoustic waves in a non-equilibrium plasma (Rosenbluth and Rostoker, 1962) and there have been several suggestions as to which mechanisms could produce the necessary ion-acoustic fluctuations. These include a current instability (e.g., Foster et al., 1988; Collis et al., 1991; Rietveld et al., 1991), an ion-ion two-stream instability (e.g., Wahlund et al., 1992) and a parametric decay of Langmuir waves (e.g., Forme, 1993, 1999). The progress of the understanding of NEIAL during the first decade since their discovery can be found in the extensive review by Sedgemore-Schulthess and St.-Maurice (2001) and the topic is still generating considerable interest (e.g, Forme et al., 2001; Grydeland et al., 2003, 2004; Strømme, 2004; Strømme et al., 2005; Kontar and Pecseli, 2005; Ogawa et al., 2006; Daldorff et al., 2007; Lunde et al., 2007; Michell et al., 2008; Sullivan et al., 2008; Lunde et al., 2009; Michell et al., 2009; Michell and Samara, 2010; Diaz et al., 2010).

Figure 6.4 exemplifies the three main categories of NEIAL mentioned above. The spectra were measured with the 42-m ESR during 2007 and the figure shows power spectral density as a function of frequency and altitude. The dataset is based on the International Polar Year experiment which had an upper altitude limit of 370 km and it can be seen that the spectral enhancement is probably present at even higher altitudes. The panels (from left to right) show 6-second integrations of respectively, an enhanced downshifted shoulder measured on 13 March 2007 at 01:53:12 UT, an enhanced upshifted shoulder measured on 5 July at 05:43:24 UT and a case of enhancement of both shoulders measured on 21 July at 04:56:42 UT.

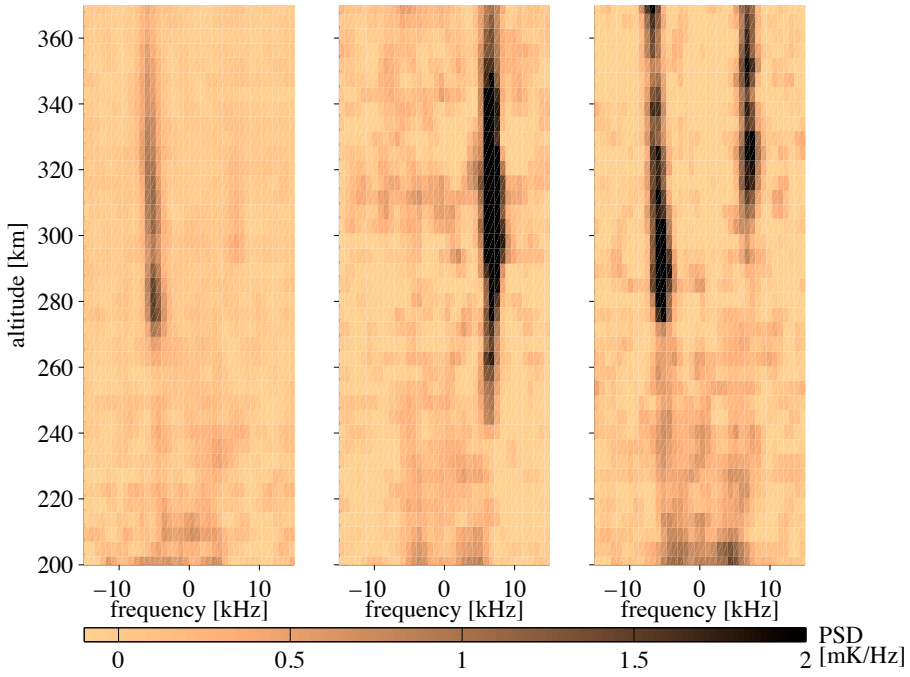

Figure 6.4. Three examples of classical NEIAL spectra measured with the 42-m ESR during 2007. The panels (from left to right) show an enhanced downshifted shoulder measured on 13 March 2007 at 01:53:12 UT, an enhanced upshifted shoulder measured on 5 July at 05:43:24 UT and a case of enhancement of both shoulders measured on 21 July 04:56:42 UT.

In Papers IV, V, and VI we address a type of ion line enhancement with other characteristics than what has so far been associated with classical NEIAL. This type of ion line enhancement, which is often localised to an altitude range of less than 20 km, located at or close to the ionospheric F region density peak, is characterised by a significant power spectral density enhancement from the downshifted ion-acoustic line to the upshifted ion-acoustic line and at all frequencies in between, such that the spectral shape is essentially conserved. Little or no asymmetry between the up- and downshifted ion line shoulders is observed

CHAPTER 7

Summary of included papers

Paper I
Dispersive MHD waves and alfvenons in charge non-neutral plasmas

Paper I describes the dispersive properties of linear and nonlinear waves in the framework of MHD, including the Hall term, electron-pressure gradients, electron inertia and space-charge effects. The paper discusses the effects of these additional terms through analytical expansions and dispersion diagrams, where the latter separate linear and nonlinear waves. The solitary waves (referred to as alfvenons in the paper) are shown to occupy two distinct regions in the phase space spanned by the wave's angle (to the magnetic field) of propagation and speed. The region of low (high) speeds constitutes wave solutions associated with positive (negative) electric potentials. Such electric potentials are related to observations by satellites in auroral regions and are postulated to exist in the solar corona.

Paper II
Electric Potentials and Energy Fluxes Available for Particle Acceleration by Alfvenons in the Solar Corona

Paper II presents solitary wave solutions (alfvenons) applicable for the solar corona. It is shown that negative electric potentials associated with fast alfvenons can accelerate electrons to several 100 keV consistent with the observed X-rays during solar flares. Slow alfvenons, on the other hand, are associated with positive potentials which could accelerate solar wind ions to 300–800 km/s.

Paper III
Heating of the Solar Corona by Dissipative Alfvén Solitons - Reply

Paper III is a reply to a comment by E. Infeld on an earlier Letter on heating of the solar corona by dissipative Alfvén solitary waves. The reply includes a calculation of the perpendicular (to the magnetic field) size of alfvénons in Hall MHD. The

estimated sizes are of the order of 1–100 km in the Earth's magnetosphere and 1–100 m in the solar corona.

Paper IV
Ion-acoustic solitary waves and spectrally uniform scattering cross section enhancements

Paper IV presents EISCAT Svalbard Radar (ESR) observations of a type of ion line enhancement which is spectrally uniform, i.e. the up- and downshifted shoulder and the spectral valley in between are enhanced equally and simultaneously. The enhancement is hereafter referred to as a spectrally uniform ion line power enhancement (SUIPE). Based on an MHD model adapted from Paper I, a theory is developed where solitary ion-acoustic waves propagating through the radar beam are shown to enhance the backscattered power by one order of magnitude above the thermal level. The predictions are confirmed by the observations.

Paper V
Soliton-induced spectrally uniform ion line power enhancements at the ionospheric *F* region peak

Paper V presents 48 cases of SUIPEs. This phenomenon was first addressed in Paper IV. The events were observed by the ESR International Polar Year experiment, which was run from March 2007 to February 2008. The spectral power ehancements were seen at altitudes between 210 km and 280 km, occur at the ionospheric F region peak and are one order of magnitude above the thermal level. These characteristics are in good agreement with the predictions of the model presented in Paper IV. The occurrence shows a clear preference for magnetically disturbed conditions, with the likelihood of occurrence increasing with increasing K index. A majority of the events occur in the magnetic evening to pre-midnight sector.

Paper VI
Incoherent scatter ion line enhancements and auroral arc-induced Kelvin-Helmholtz turbulence

Paper VI presents two cases of SUIPEs in conjunction with auroral arcs drifting through the ESR beam at a speed of 4.3 km/s and 1.6 km/s, respectively. The auroral arc passages are preceded by significantly enhanced ion temperatures in the E region, which are shown to generate high velocity shears perpendicular to the geomagnetic field and give rise to a growing Kelvin-Helmholtz instability in the F region. The paper assesses the possibility that the low-frequency turbulence associated with the Kelvin-Helmholtz instability can explain the characteristics of the observed ion line enhancements.

Acknowledgements

I would like to thank my supervisors Lars Eliasson and Kristof Stasiewicz. Lars, in an otherwise often tight time schedule, you have always tried to make time for dealing with any issues that arose and for helping me facing my challenges during these years. Kristof, you encouraged me twice to explore the world of plasma physics and generously offered your guidance along the way.

I am thankful to Evgenia Belova for inviting me to IRF and for introducing me to the scientific process and to the National Graduate School of Space Technology for partly funding this work.

From Gudmund Wannberg, I have learnt a lot on how incoherent scatterers perceive the ionospheric plasma environment, and he has also generously shared a good deal of understanding during tough times. In short, you have been of great help in so many ways. Thank you very much!

Tima Sergienko has been a great asset throughout this whole period and I am truly grateful for your patience and never-ending willingness to discuss various concepts in plasma physics. I am also grateful to Ingemar Häggström for help in dealing with radar data and to Sheila Kirkwood for sharing her view on what going for a PhD is all about. Many thanks also go to Roshny Ajil and Rick McGregor for valuable corrections and improvements of the manuscript.

Thank you Mats Holmström and Thomas Leyser for sincere interest and scientific advice.

Without Carina Gunillasson's willingness to think outside the box, Mats Luspa's, Stefan Vanhaniemi's and Leif Kalla's inexhaustible readiness to help with computer-related issues and Birgitta Määttä's assistance in the library, this journey would have been much less smooth. To everyone at IRF, not mentioned here by name, thank you all for the ways in which you have helped and contributed to this thesis and for constituting the healthy mix of people that has offered such rich possibilities for self-improvement and personal growth.

Besides being part of IRF as a whole, it has been a privilege to conduct the studies in company of several other PhD students and I am grateful for all the ways in which you have enriched my time at IRF, both at work and outside the office. One of them, Martin Waara, has accompanied me along almost the whole PhD student path. Always up for listening, discussing, and giving your opinions on different matters, big or small, you have been of great importance and I am

truly grateful to you for this period of time.

Several former colleagues and friends have moved on to new challenges, but many positive memories remain. It makes me happy to think about long talks during endless drives with Tony T. Giang, game evenings and trips with Csilla Szasz and Johan Kero, happenings organised by Andreas Ekenbäck and David McCann and the shared enjoyment of snow and Indian food with Ajil Kottayil and K Satheesan.

I would also like to express a special gratitude to Kiruna and what she has come to represent for me. After all, she was a big reason for me finding my way to IRF in the first place.

Kiruna Karate Kai has been a truly essential part of my life during these years and it has meant everything to be part of such a remarkable group of people. Ronnie Pettersson and all the members, OSU!

Mats Stridsman, Helena Nilsson, and Sandra Niemi Nilsson showed tremendous hospitality and generosity during several of my stays in Kiruna. I will always treasure those months, thank you!

I want to thank friends and family and I am especially grateful to my mother for continuous encouragement and for your insights on different approaches to life. It may not have been always easy to accept, but there was always something to learn. I am grateful to Hans Johansson for your sincere interest and sound perspective on things.

Finally, a heartfelt thank you to Meike for your love, support and patience. I see that it was not an easy task to stand beside and ask the "right" questions. "Som en gummiboll...".

Västerås, April 2011

Bibliography

Alfvén, H. (1942). Existence of electromagnetic-hydromagnetic waves. *Nature*, *150*(3805), 405–406.

Alfvén, H. (1953). *Cosmical Electrodynamics*, The International Series of Monographs on Physics, Oxford: University Press.

Alfvén, H. (1976). On Frozen-In Field Lines and Field-Line Reconnection. *J. Geophys. Res.*, *81*(22), 4019–4021.

Appleton, E. V. & Barnett, M. A. F. (1926). On some direct evidence for downward atmospheric reflection of electric rays. *Proc. Roy. Soc.*, *109*, 621–641.

Bauer, P. (1975). Theory of waves incoherently scattered. *Phil. Trans. Roy. Soc. London A.*, *280*(1293), 167–191.

Bellan, P. M. (2006). *Fundamentals of Plasma Physics*, Cambridge: University Press. ISBN 13-978-0-521-82116-2.

Bohm, D. & Gross, E. P. (1949). Theory of Plasma Oscillations. A. Origin of Medium-Like Behavior. *Phys. Rev.*, *75*(12), 1851–1864.

Bowles, K. L. (1958). Observations of vertical-incidence scatter from the ionosphere at 41 Mc/s. *Phys. Rev. Lett.*, *1*, 454–455.

Buchert, S. C., van Eyken, A. P., Ogawa, T., & Watanabe, S. (1999). Naturally enhanced ion-acoustic lines seen with the EISCAT svalbard radar. *Adv. Space Res.*, *23*, 1699–1704.

Budden, K. G. (1985). *The propagation of radio waves*, Cambridge: Cambridge University Press. ISBN 0-521-25461-2.

Bulanov, S. V., Pegoraro, F., & Sakharov, A. S. (1992). Magnetic reconnection in electron magnetohydrodynamics. *Phys. Fluids. B*, *4*(8), 2499–2508.

Buneman, O. (1962). Scattering of Radiation by the Fluctuations in a Nonequilibrium Plasma. *J. Geophys. Res.*, *67*, 2050–2053.

Chen, F. F. (1984). *Introduction to Plasma Physics and Controlled Fusion*, 2nd ed., New York: Plenum Press.

Clemmow, P. C. & Dougherty, J. P. (1969). *Electrodynamics of Particles and Plasmas*, Reading: Addison-Wesley. ISBN 978-0201011432.

Collis, P. N., Häggström, I., Kaila, K., & Rietveld, M. T. (1991). EISCAT radar observations of enhanced incoherent scatter spectra: Their relation to red aurora and field-aligned currents. *Geophys. Res. Lett.*, *18*, 1031–1034.

Courtillot, V. & Le Mouel, J. L. (1988). Time variations of the Earth's magnetic field: From daily to secular. *Annual Rev. Earth Plan. Sci.*, *16*, 389–476.

Daldorff, L. K. S., Pécseli, H. L., & Trulsen, J. (2007). Nonlinearly generated plasma waves as a model for enhanced ion acoustic lines in the ionosphere. *Geophys. Res. Lett.*, *34*, L18 101.

Debye, P. & Hückel, E. (1923). The theory of electrolytes I. The lowering of the freezing point and related occurences. *Physik. Zeits.*, *24*, 185–206.

Diaz, M. A., Semeter, J. L., Oppenheim, M., & Zettergren, M. (2010). Analysis of beam plasma instability effects on incoherent scatter spectra. *Ann. Geophys.*, *28*(12), 2169–2175.

Dougherty, J. P. & Farley, D. T. (1960). A Theory of Incoherent Scattering of Radio Waves by a Plasma II. Scattering in a Magnetic Field. *Proc. Roy. Soc. London A.*, *259*(1296), 79–99.

Dubinin, E., Sauer, K., McKenzie, J. F., & Chanteur, G. (2003). Solitons, oscillitons, and stationary waves in a cold p - α plasma. *J. Geophys. Res.*, *108*, 1295.

Dupree, T. H. (1963). Kinetic theory of plasma and the electromagnetic field. *Phys. Fluids*, *6*(12), 1714–1729.

Ekeberg, J., Wannberg, G., Eliasson, L., & Stasiewicz, K. (2010). Ion-acoustic solitary waves and spectrally uniform scattering cross section enhancements. *Ann. Geophys.*, *28*(6), 1299–1306.

Ekeberg, J., Stasiewicz, K., Wannberg, G., Sergienko, T., & Eliasson, L. (2011a). Incoherent scatter ion line enhancements and auroral arc-induced Kelvin-Helmholtz turbulence. Submitted to *J. Atmos. Solar-Terr. Phys*.

Ekeberg, J., Wannberg, G., Eliasson, L., & Häggström, I. (2011b). Soliton-induced spectrally uniform ion line power enhancements at the ionospheric *F* region peak. Submitted to *Earth Planets Space*.

Engwall, E. (2009). *Low-Energy Ion Escape from the Terrestrial Polar Regions*, Ph.D. thesis, Uppsala University. ISBN 978-91-554-7512-3.

Evans, J. V. (1975). High-power radar studies of the ionosphere. *Proc. IEEE*, *63*, 1636–1650.

Fälthammar, C.-G. (1999). *Space Physics*, 2 ed., Lecture notes, Stockholm: Royal Institute of Technology.

Fejer, J. A. (1960). Scattering of radio waves by an ionized gas in thermal equilibrium. *Can. J. Phys.*, *38*(8), 1114–1133.

Forme, F., Ogawa, Y., & Buchert, S. C. (2001). Naturally enhanced ion acoustic fluctuations seen at different wavelengths. *J. Geophys. Res.*, *106*, 21 503–21 516.

Forme, F. R. E. (1993). A new interpretation of the origin of enhanced ion acoustic fluctuations in the upper ionosphere. *Geophys. Res. Lett.*, *20*, 2347–2350.

Forme, F. R. E. (1999). Parametric decay of beam-driven Langmuir wave and enhanced ion-acoustic fluctuations in the ionosphere: a weak turbulence approach. *Ann. Geophys.*, *17*, 1172–1181.

Foster, J. C., del Pozo, C., Groves, K., & St-Maurice, J. P. (1988). Radar observations of the onset of current-driven instabilities in the topside ionosphere. *Geophys. Res. Lett.*, *15*, 160–163.

Froula, D. H., Glenzer, S. H., Luhmann Jr., N. C., & Sheffield, J. (2011). *Plasma Scattering of Electromagnetic Radiation: Theory and Mesurement Techniques*, 2 ed., New York: Academic Press. ISBN 978-0-12-374877-5.

Gauss, C. F. (1838). Allgemeine Theorie des Erdmagnetismus, in *Resultate aus den Beobachtungen des magnetischen Vereins im Jahre 1838*, edited by Gauss, C. F. & Weber, W., pp. 1–57, Leipzig.

Gordon, W. E. (1958). Incoherent scattering of radio waves by free electrons with applications to space exploration by radar. *Proc. Inst. Radio Engrs.*, *46*, 1824–1829.

Grydeland, T., La Hoz, C., Hagfors, T., Blixt, E. M., Saito, S., Strømme, A., & Brekke, A. (2003). Interferometric observations of filamentary structures associated with plasma instability in the auroral ionosphere. *Geophys. Res. Lett.*, *30*(6), 060 000–1.

Grydeland, T., Blixt, E., Løvhaug, U., Hagfors, T., La Hoz, C., & Trondsen, T. (2004). Interferometric radar observations of filamented structures due to plasma instabilities and their relation to dynamic auroral rays. *Ann. Geophys.*, *22*, 1115–1132.

Hagfors, T. (1960). *Density fluctuations in a plasma in a magnetic field, with applications to the ionosphere*, Scientific rept. No. 1, Stanford Electronics Laboratories.

Hassam, A. B. & Huba, J. D. (1987). Structuring of the AMPTE magnetotail barium releases. *Geophys. Res. Lett.*, *14*(1), 60–63.

Hassam, A. B. & Huba, J. D. (1988). Magnetohydrodynamic equations for systems with large Larmor radius. *Phys. Fluids*, *31*(2), 318–325.

Hassam, A. B. & Lee, Y. C. (1984). Drift-ideal magnetohydrodynamics. *Phys. Fluids*, *27*(2), 438–446.

Heaviside, O. (1902). Telegraphy I, Theory, in *Encycl. Britannica*, vol. 33, pp. 213–218, Edinburgh, 10 ed.

Huba, J. D. (1991). Theory and simulation of a high-frequency magnetic drift wave. *Phys. Fluids. B*, *3*(12), 3217–3225.

Huba, J. D. (2003). Hall Magnetohydrodynamics: A Tutorial, in *Space Plasma Simulation*, edited by Büchner, J., Dum, C. T., & Scholer, M., Lecture Notes in Physics, pp. 166–192, Heidelberg: Springer-Verlag.

Jackson, J. D. (1999). *Classical electrodynamics*, 3rd ed., New York: John Wiley & Sons. ISBN 0-471-30932-X.

Kahn, F. D. (1959). Long-range interactions in ionized gases in thermal equilibrium. *Astrophys. J.*, *129*(1), 205–216.

Kelley, M. C. (1989). *The Earth's Ionosphere*, San Diego: Academic Press. ISBN 0-12-404013-6.

Kennelly, A. E. (1902). On the elevation of the electrically conducting strata of the Earth's atmosphere. *Elec. World Eng.*, *39*, 473.

Kikuchi, K., Barakat, A., & St-Maurice, J. (1989). Monte Carlo computations of *F*-region incoherent radar spectra at high latitudes and the use of a simple method for non-Maxwellian spectral calculations. *Ann. Geophys.*, *7*, 183–194.

Kingsep, A. S., Chukbar, K. V., & Yan'kov, V. V. (1990). Electron Magnetohydrodynamics, in *Reviews of Plasma Physics*, edited by Kadomtsev, A. A., vol. 16, p. 243, New York: Consultants Bureau.

Klimontovich, Y. L. (1967). *The Statistical Theory of Non-Equilibrium Processes in a Plasma*, vol. 11 of International series of monographs in natural philosophy, Oxford: Pergamon Press.

Kontar, E. P. & Pecseli, H. L. (2005). Nonlinear wave interactions as a model for naturally enhanced ion acoustic lines in the ionosphere. *Geophys. Res. Lett.*, *32*(5).

Krall, N. A. & Trivelpiece, A. W. (1973). *Principles of Plasma Physics*, International series in pure and applied physics, New York: McGraw-Hill. ISBN 0-07-035346-8.

Langmuir, I. (1928). Oscillations in ionized gases. *P. Natl. Acad. Sci.*, *14*, 627–637.

Lehtinen, M. S. & Huuskonen, A. (1996). General incoherent scatter analysis and GUISDAP. *J. Atmos. Terr. Phys.*, *58*, 435–452.

Lord Rayleigh. (1906). On electrical vibrations and the constitution of the atom. *Phil. Mag.*, *11*, 117–123.

Lunde, J., Gustavsson, B., Løvhaug, U. P., Lorentzen, D. A., & Ogawa, Y. (2007). Particle precipitations during NEIAL events: simultaneous ground based observations at Svalbard. *Ann. Geophys.*, *25*(6), 1323–1336.

Lunde, J., Løvhaug, U. P., & Gustavsson, B. (2009). Particle precipitation during NEIAL events: simultaneous ground based nighttime observations at Svalbard. *Ann. Geophys.*, *27*(5), 2001–2010.

Mandl, F. (1988). *Statistical Physics*, 2nd ed., The Manchester physics series, Chichester: John Wiley & Sons. ISBN 978-0-471-91533-1.

Marconi, G. (1902a). The progress of electric space telegraphy. *Electrician*, *49*, 388–392.

Marconi, G. (1902b). The progress of electric space telegraphy. *Proc. Roy. Inst.*, *17*, 195–210.

Marconi, G. (1902c). Note on the effect of daylight on the propagation of electrmagnetic impulses over long distances. *Proc. Roy. Soc.*, *71*, 344–347.

Michell, R. G. & Samara, M. (2010). High-resolution observations of naturally enhanced ion acoustic lines and accompanying auroral fine structures. *J. Geophys. Res.*, *115*, 3310.

Michell, R. G., Lynch, K. A., Heinselman, C. J., & Stenbaek-Nielsen, H. C. (2008). PFISR nightside observations of naturally enhanced ion acoustic lines, and their relation to boundary auroral features. *Ann. Geophys.*, *26*(11), 3623–3639.

Michell, R. G., Lynch, K. A., Heinselman, C. J., & Stenbaek-Nielsen, H. C. (2009). High time resolution PFISR and optical observations of naturally enhanced ion acoustic lines. *Ann. Geophys.*, *27*(4), 1457–1467.

Nordling, C. & Österman, J. (1996). *Physics Handbook for Science and Engineering*, 5th ed., Lund: Studentlitteratur. ISBN 91-44-16575-7.

Ogawa, Y., Buchert, S. C., Fujii, R., Nozawa, S., & Forme, F. (2006). Naturally enhanced ion-acoustic lines at high altitudes. *Ann. Geophys.*, *24*, 3351–3364.

Raman, R. S. V., St-Maurice, J. P., & Ong, R. S. B. (1981). Incoherent scattering of radar waves in the auroral ionosphere. *J. Geophys. Res.*, *86*, 4751–4762.

Renau, J. (1960). Scattering of Electromagnetic Waves from a Nondegenerate Ionized Gas. *J. Geophys. Res.*, *65*(11), 3631–3640.

Rietveld, M. T., Collis, P. N., & St-Maurice, J. P. (1991). Naturally enhanced ion-acoustic waves in the auroral ionosphere observed with the EISCAT 933 MHz radar. *J. Geophys. Res.*, *96*, 19 291–19 305.

Roberts, K. V. & Taylor, J. B. (1962). Magnetohydrodynamic Equations for Finite Larmor Radius. *Phys. Rev. Lett.*, *8*(5), 197–198.

Rosenbluth, M. N. & Rostoker, N. (1962). Scattering of Electromagnetic Waves by a Nonequilibrium Plasma. *Phys. Fluids*, *5*, 776–788.

Rostoker, N. (1964a). Test Particles in a Completely Ionized Plasma. *Phys. Fluids*, *3*(1), 1–14.

Rostoker, N. (1964b). Superposition of Dressed Test Particles. *Phys. Fluids*, *7*(4), 479–490.

Rostoker, N. (1964c). Test Particle Method in Kinetic Theory of a Plasma. *Phys. Fluids*, *7*(4), 491–498.

Salpeter, E. E. (1960). Electron density fluctuations in a plasma. *Phys. Rev.*, *120*(5), 1528–1535.

Sauer, K., Dubinin, E., & McKenzie, J. (2001). New type of soliton in bi-ion plasmas and possible implications. *Geophys. Res. Lett.*, *28*(18), 3589.

Sauer, K., Dubinin, E., & McKenzie, J. (2003). Solitons and oscillitons in multi-ion space plasmas. *Nonlinear Proc. Geophys.*, *10*, 121.

Sedgemore-Schulthess, F. & St.-Maurice, J. (2001). Naturally Enhanced Ion-Acoustic Spectra and Their Interpretation. *Surveys in Geophys.*, *22*(1), 55–92.

Sheffield, J. (1975). *Plasma Scattering of Electromagnetic Radiation*, New York: Academic Press. ISBN 0-12-638750-8.

Stasiewicz, K. (2004). Theory and observations of slow-mode solitons in space plasmas. *Phys. Rev. Lett.*, *93*(12), 125 004.

Stasiewicz, K. (2005). Nonlinear Alfvén, magnetosonic, sound, and electron inertial waves in fluid formalism. *J. Geophys. Res.*, *110*, A03 220.

Stasiewicz, K. & Ekeberg, J. (2007). Heating of the Solar Corona by Dissipative Alfvén Solitons - Reply. *Phys. Rev. Lett.*, *99*(8), 89 502.

Stasiewicz, K. & Ekeberg, J. (2008a). Electric Potentials and Energy Fluxes Available for Particle Acceleration by Alfvenons in the Solar Corona. *Astrophys. J. Lett.*, *680*, L153–L156.

Stasiewicz, K. & Ekeberg, J. (2008b). Dispersive MHD waves and alfvenons in charge non-neutral plasmas. *Nonlin. Proc. Geophys.*, *15*, 681–693.

Stewart, B. (1882). Hypothetical views regarding the connection between the state of the sun and terrestrial magnetism, in *Encycl. Britannica*, vol. 16, pp. 181–184, Edinburgh, 9 ed.

Strømme, A. (2004). *Naturally Enhanced Wave Modes Observed with the EISCAT Svalbard Radar*, Ph.D. thesis, Department of Physics, University of Tromsø.

Strømme, A., Belyey, V., Grydeland, T., La Hoz, C., Løvhaug, U. P., & Isham, B. (2005). Evidence of naturally occurring wave-wave interactions in the polar ionosphere and its relation to naturally enhanced ion acoustic lines. *Geophys. Res. Lett.*, *32*(5).

Sullivan, J. M., Lockwood, M., Lanchester, B. S., Kontar, E. P., Ivchenko, N., Dahlgren, H., & Whiter, D. K. (2008). An optical study of multiple NEIAL events driven by low energy electron precipitation. *Ann. Geophys.*, *26*(8), 2435–2447.

Tonks, L. & Langmuir, I. (1929). Oscillations in ionized gases. *Phys. Rev.*, *33*, 195–211.

Wahlund, J.-E., Forme, F. R. E., Opgenoorth, H. J., Persson, M. A. L., Mishin, E. V., & Volokitin, A. S. (1992). Scattering of electromagnetic waves from a plasma: Enhanced ion acoustic fluctuations due to ion-ion two-stream instabilities. *Geophys. Res. Lett.*, *19*, 1919–1922.

Wannberg, G., Wolf, I., Vanhainen, L.-G., Koskenniemi, K., Röttger, J., Postila, M., Markkanen, J., Jacobsen, R., Stenberg, A., Larsen, R., Eliassen, S., Heck, S., & Huuskonen, A. (1997). The EISCAT Svalbard radar: A case study in modern incoherent scatter radar system design. *Radio Sci.*, *32*, 2283–2308.

Weinstock, J. (1965). New Approach to the Theory of Fluctuations in a Plasma. *Phys. Rev.*, *139*(2A), A388–A393.

Weinstock, J. (1967). Correlation Functions and Scattering of Electromagnetic Waves by Inhomogeneous and Nonstationary Plasmas. *Phys. Fluids*, *10*(9), 2065–2072.

IRF Scientific Report 301
ISSN 0284-1703
ISBN 978-91-977255-7-6

Institutet för rymdfysik
Swedish Institute of Space Physics